

ARTICLE

Received 7 Jan 2016 | Accepted 16 Sep 2016 | Published 8 Nov 2016

DOI: [10.1038/ncomms13276](https://doi.org/10.1038/ncomms13276)

OPEN

Random synaptic feedback weights support error backpropagation for deep learning

Timothy P. Lillicrap^{1,2}, Daniel Cownden³, Douglas B. Tweed^{4,5} & Colin J. Akerman¹

The brain processes information through multiple layers of neurons. This deep architecture is representationally powerful, but complicates learning because it is difficult to identify the responsible neurons when a mistake is made. In machine learning, the backpropagation algorithm assigns blame by multiplying error signals with all the synaptic weights on each neuron's axon and further downstream. However, this involves a precise, symmetric backward connectivity pattern, which is thought to be impossible in the brain. Here we demonstrate that this strong architectural constraint is not required for effective error propagation. We present a surprisingly simple mechanism that assigns blame by multiplying errors by even random synaptic weights. This mechanism can transmit teaching signals across multiple layers of neurons and performs as effectively as backpropagation on a variety of tasks. Our results help reopen questions about how the brain could use error signals and dispel long-held assumptions about algorithmic constraints on learning.

¹ Department of Pharmacology, University of Oxford, Oxford OX1 3QT, UK. ² Google DeepMind, 5 New Street Square, London EC4A 3TW, UK. ³ School of Biology, University of St Andrews, Harold Mitchel Building, St Andrews, Fife KY16 9TH, UK. ⁴ Departments of Physiology and Medicine, University of Toronto, Toronto, Ontario M5S 1A8, Canada. ⁵ Centre for Vision Research, York University, Toronto, Ontario M3J 1P3, Canada. Correspondence and requests for materials should be addressed to T.P.L. (email: timothylillicrap@google.com) or to C.J.A. (email: colin.akerman@pharm.ox.ac.uk).

Neuro networks in the brain compute via multiple layers of interconnected neurons. During learning, these neurons are believed to adjust their synapses so that the network's outputs become more appropriate for its tasks. In many cases, learning is thought to utilize error signals, such as those that result from mismatches between expected and actual perceptions, or between intended and realized motor behaviours^{1–8}. This requires mechanisms that can adjust the weights of synapses earlier in a network (for example, the synapse between x_i and h_j in Fig. 1a) on the basis of downstream errors (for example, e in Fig. 1a).

Naive learning rules could adjust synapses deep within a network based on the correlations between a scalar error signal and the neuronal activity⁹. However, the performance of such learning rules slows significantly as the size of a network grows^{10,11}. The reason for this is that as the number of neurons in a network increases, so does the variance in estimates of a neuron's contribution to the error¹². More powerful learning rules could send specific teaching signals to a neuron based on how that neuron contributed to the error¹³. In artificial intelligence an algorithm called backpropagation of error (backprop) is used to assign error on a neuron-by-neuron basis¹⁴ (Fig. 1a). Backprop works well in real-world applications, underlies recent advances in reinforcement and unsupervised learning^{15–17}, and can account for cell responses in some areas of cortex^{18–20}. But, for a variety of reasons, it has been difficult to imagine how a learning algorithm such as backprop could be implemented by neural circuits in the brain^{21,22}.

One of the most significant issues is that backprop requires that the downstream errors are fed back to upstream neurons via an exact, symmetric copy of the downstream synaptic weight matrix^{11,13,21–27}. More precisely, backprop multiplies error signals e by the weight matrix W^T , which is the transpose of the forward synaptic connections, W (Fig. 1b). This issue was described in detail by Grossberg, who named it the weight transport problem²². The name arises from the fact that for each neuron, information about downstream synaptic weights must be 'transported' to make optimal updates to the neurons incoming (forward) synaptic weights. Backprop requires each neuron hidden deep within the network to have precise knowledge of all of its downstream synapses, since the error signal arriving at a hidden unit must be multiplied by the strength of that neuron's forward synaptic connections to the source of the error. Weight transport was also identified as a major problem by Zipser and Rumelhart²⁴, and their concerns were echoed by Crick²¹ who noted that, when taken at face value, backprop seems to require rapid information transfer back along axons from each of its synaptic outputs.

A number of studies have suggested potential solutions to the weight transport problem. Indeed, encouraged by initial empirical observations, several theoretical studies examined the possibility that backprop might in fact be implemented via the retrograde transmission of information along axons²⁸. However, further empirical work has shown that retrograde transport operates on timescales that are orders of magnitude slower than forward propagating neural activity, making it fundamentally unable to support backprop-like learning²⁶. As an alternative to sending error information anterogradely, it has been suggested that errors could instead be fed back through a second network^{4,21,23–25,29–32}. However, most of these approaches either assume that forward and feedback connections are symmetric, or they propose more intricate learning rules for the backward weights that maintain precise symmetry. These approaches to the weight transport problem have helped to perpetuate the view that to achieve backprop-like learning performance, the brain would have to exhibit precise symmetric

connectivity between upstream and downstream neurons. And whilst the brain does exhibit widespread reciprocal connectivity that would be consistent with the transfer of error information across layers, it is not believed to exhibit such precise patterns of reciprocal connectivity²¹.

Here we have re-examined the conditions under which a network can exhibit backprop-like learning. We find that the precise symmetric connectivity between connected layers assumed by backprop is simply not required to obtain quick learning. Surprisingly, we show that even fixed, random connectivity patterns can suffice. Without adjusting any feedback connections, we show that implicit dynamics in the standard forward weight updates encourage a soft alignment between the forward and backward weights, allowing effective flow of neuron-by-neuron error signals across multiple layers. This simple mechanism avoids all transport of synaptic weight

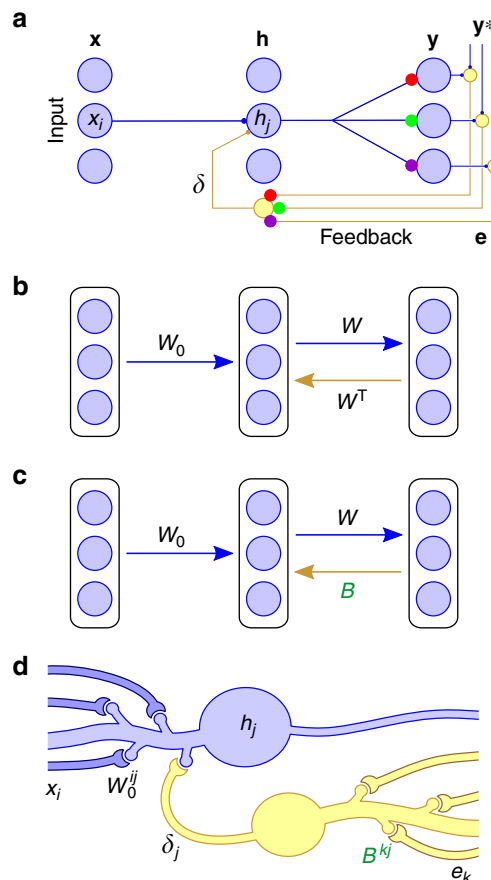


Figure 1 | Random feedback weights can deliver useful teaching signals. (a) The backprop learning algorithm requires that neurons know each others' synaptic weights, for example, the three coloured synapses on the feedback cell at the bottom must have weights equal to those of the corresponding coloured synapses in the forward path. (b) Backprop computes teaching, or modulator, vectors by multiplying the error vector e by the transpose of the forward weight matrix W ; that is, $\delta_{BP} = W^T e$. (c) Our feedback alignment method replaces W^T with a matrix of fixed random weights, B , so that $\delta_{FA} = Be$. Thus, each neuron in the hidden layer receives a random projection of the error vector. (d) Potential synaptic circuitry underlying feedback alignment, shown for a single hidden unit (matrix superscripts denote single synapses, see main text for further explanation). This diagram is provided for illustrative purposes. There are many possible configurations that could support learning with feedback alignment, or algorithms like it, and it is this structural flexibility that we believe is important.

information and does so despite achieving only a modest symmetry in reciprocal connectivity. Of course, these observations are compatible with the possibility that the brain makes use of more intricate architectures, or more complex algorithms. Our results also leave open many questions about how the brain might implement fast error-driven learning. Importantly however, they reveal much lower architectural constraints on what is required for effective error propagation across multiple layers of neurons.

Results

Random feedback weights can deliver useful teaching signals.

A fundamental question in neuroscience is how upstream synapses (for example, the synapses between x_i and h_j in Fig. 1a) might be adjusted on the basis of downstream errors (for example, e in Fig. 1a). The learning algorithm backprop computes gradients of the performance, that is, the loss, for each of the synapses in the network and uses these gradients to update the synaptic weights. Specifically, backprop computes feedback by multiplying error signals e by the weight matrix W^T , which is the transpose of the forward synaptic connections W . This means that feedback neurons would somehow have to know all the synaptic weights W in the forward pathway. Here we describe a new deep learning algorithm that is fast and accurate, like backprop, but much simpler as it avoids all transport of synaptic weight information. Our aim is to describe this novel algorithm and its potential relevance in as simple a form as possible, meaning that we overlook aspects of neurophysiology that will ultimately be relevant for a complete view of error-driven learning in the brain.

Our algorithm is based on three insights: (i) the feedback weights need not be exactly W^T . In fact, any matrix B will suffice, so long as on average, $e^T W B e > 0$, where e is the error in the network's output (Fig. 1a). Geometrically, this means the teaching signal sent by the matrix, $B e$, lies within 90° of the signal used by backprop, $W^T e$, that is, B pushes the network in roughly the same direction as backprop would. To learn with any speed though, we need better agreement between B and W^T . (ii) To end, the network could evolve to bring B and W^T into alignment. The obvious option is to adjust B , but (iii) another possibility is to do the same by adjusting W . We will show this can be achieved very simply, even with a fixed, random B (Fig. 1c). Indeed, our simulations suggest that this is a minimal requirement and that there may be many ways to achieve the same effects.

For clarity, we first considered a three-layer network of linear neurons. The network's output is $y = Wh$, where h is the hidden-unit activity vector, given by $h = W_0x$, where x is the input to the network. W_0 is the matrix of synaptic weights

from x to h , and W is the weights from h to y . The network learns to approximate a linear function, T (for 'target'). Its goal is to reduce the squared error, or loss, $\mathcal{L} = \frac{1}{2}e^T e$, where the error $e = y^* - y = Tx - y$. To train this network, backprop would adjust all the weights down the gradient of the loss, that is, $\Delta W \propto \partial \mathcal{L} / \partial W = -e h^T$, and $\Delta W_0 \propto \partial \mathcal{L} / \partial W_0 = (\partial \mathcal{L} / \partial h)(\partial h / \partial W_0) = -W^T e x^T$. Our new algorithm adjusts W in the same way as backprop, but for W_0 it uses a simpler formula, which needs no information about W or any other synapses but instead sends e through a fixed random matrix B

$$\Delta W_0 \propto B e x^T, \quad (1)$$

We call this algorithm **feedback alignment**. To illustrate the algorithm's performance, we describe an abstract version of a simple circuit that can learn via feedback alignment. Equation (1) implies that the error vector e is carried via a set of axons that pass through an array B of synapses to yield the vector, $B e$. We will also refer to the vector $B e$ as δ , or the modulator signal, because axon branches carrying δ contact hidden-layer neurons to modulate their learning (Fig. 1d). For instance, neuron j receives the signal δ_j (the j -th element of δ), and the weight change in synapse i onto neuron j is proportional to the product of δ_j and the input x_i to that synapse (and a simple function of the activity of the output neuron in the nonlinear case, see below). Therefore, the mechanism can require as few as one modulator signal per learning cell, which influences plasticity at its incoming forward synapses. In the simple models that we examine, the delivered δ_{FA} signal does not impact the forward pass post-synaptic activity, but instead acts to alter plasticity at the forward synapses. There are various ways that such a decoupling of forward and backward activity might occur in the brain, including via inputs that arrive at different times or to different subcellular compartments^{33–36}, or via different types of synapse^{37,38}. More complex models may involve forward and backward pathways that interact via the post-synaptic voltage, possibly to allow inference and learning processes to interact (see Discussion).

We will first demonstrate that this circuit learns by encouraging a soft alignment of W with B^T and then discuss why it works. Four learning algorithms were compared on a function-fitting task using a linear three-layer network (Fig. 2a; see Methods, Supplementary Note 1 and Supplementary Figs 1–4). With shallow learning, only the output weights, W , are adjusted, and the result is that the loss hardly decreases. With a fast form of reinforcement learning that delivers the same reward to each neuron, both W_0 and W are adjusted, but the learning is slow. In contrast, backprop sends the loss rapidly towards zero. Remarkably, feedback alignment does

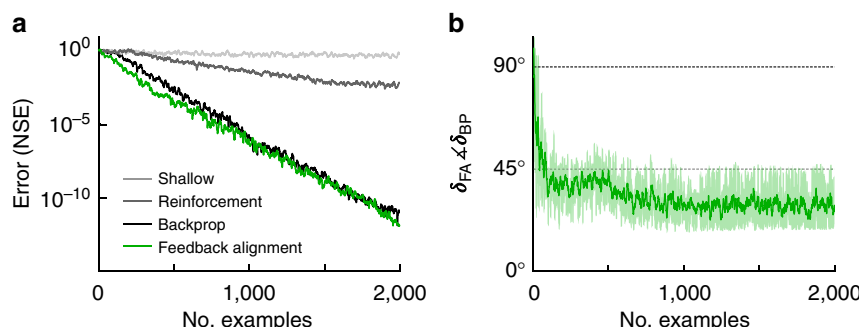


Figure 2 | Feedback alignment matches backprop performance on a linear problem. (a) Four algorithms learn to mimic a linear function: 'shallow' learning (light grey); reinforcement learning (dark grey); backprop (black); and feedback alignment (green). NSE is normalized squared error (see Methods). (b) The angle between modulator vectors prescribed by feedback alignment and backprop, δ_{FA} and δ_{BP} , decreases. Error bars are two s.d.'s for a sliding window of 10 examples.

the same and just as quickly. To explore why, we plot the angle between the modulator vector prescribed by feedback alignment, $\delta_{FA} = Be$, and the one prescribed by backprop, $\delta_{BP} = W^T e$ (Fig. 2b). Initially the angle is $\sim 90^\circ$. However, the angle soon shrinks because, even though it is fixed, B starts acting like W^T . In this way, the random feedback weights B come to transmit useful teaching signals. Notably, although the angle decreases, it never reaches zero. This highlights that even when the angle is non-zero, feedback alignment can still obtain similar levels of performance to backprop. Thus, it is not the case that error feedback must happen via precise, symmetric backward connectivity.

Feedback alignment learns under a variety of conditions.

Having examined a simple linear problem, we wanted to test whether feedback alignment could also work with nonlinear neurons in which synaptic changes depend on the post-synaptic neuron's activity, as well as on the pre-synaptic activity and modulator signal. In this case, a hidden unit with output h_j and sigmoid nonlinearity will update its incoming synaptic weights by the three-factor formula $\Delta W_0^{ij} = \delta_j x_i h'_j$, where h'_j is a simple function of the post-synaptic activity (see Methods). Nonlinear feedback alignment was tested on a benchmark problem of learning to recognize handwritten digits (Fig. 3a; see Methods). On this task, backprop brings the mean error on the test set to 2.4%, averaged over 20 runs. Feedback alignment learns just as quickly, achieving 2.1% mean error, and develops similar feature detectors (Supplementary Fig. 5). In these nonlinear experiments the modulator signals δ_{FA} and δ_{BP} also quickly align and remain stable over time (Fig. 3b). Even when we randomly remove 50% of the elements of the W and B matrices, so that neurons in \mathbf{h} and \mathbf{y} have a 25% chance of

reciprocal connection, feedback alignment still matches backprop (2.4% mean error; $n=20$; Supplementary Fig. 5). These tests support the conclusions from the simple linear case, and show that feedback alignment is robust in the case of nonlinearities and can function effectively with categorical errors, as well as with regression errors.

Processing in the brain often involves more than three layers of neurons and theoretical studies have shown that these deeper networks are better at many learning tasks³⁹. Our experiments in deeper networks reveal that feedback alignment can train deep networks by sending δ signals to multiple hidden layers. In a four-layer network for instance, axons carrying the error vector e pass through synapses B_2 to yield $\delta_2 = B_2 e$ (Fig. 3c). Axons carrying δ_2 send branches to cells of hidden layer 2 to modulate their learning, and also pass through weight array, B_1 , to yield $\delta_1 = B_1 \delta_2$. Tested on a function fitting task with a four-layer network, feedback alignment performed as well as backprop (Fig. 3d). And both feedback alignment (t -test, $n=20$, $P=9 \times 10^{-13}$) and backprop ($P=3 \times 10^{-12}$) delivered better performance with a four-layer network than with a three-layer network. Control experiments in which we froze the first layer of weights, W_0 , confirmed that feedback alignment takes advantage of depth by making effective weight updates in the deeper layers (Supplementary Notes 2 and 3 and Supplementary Fig. 6). Thus, feedback alignment, like backprop, can exploit the power of deeper networks.

So far we have shown that feedback alignment can operate in relatively small, simple networks. Next, we were interested in testing whether feedback alignment's operation can apply in more complex settings, such as in larger networks with neurons that integrate their activity over time and spike stochastically, and where the forward and feedback pathways operate synchronously. We therefore applied feedback alignment once again to the

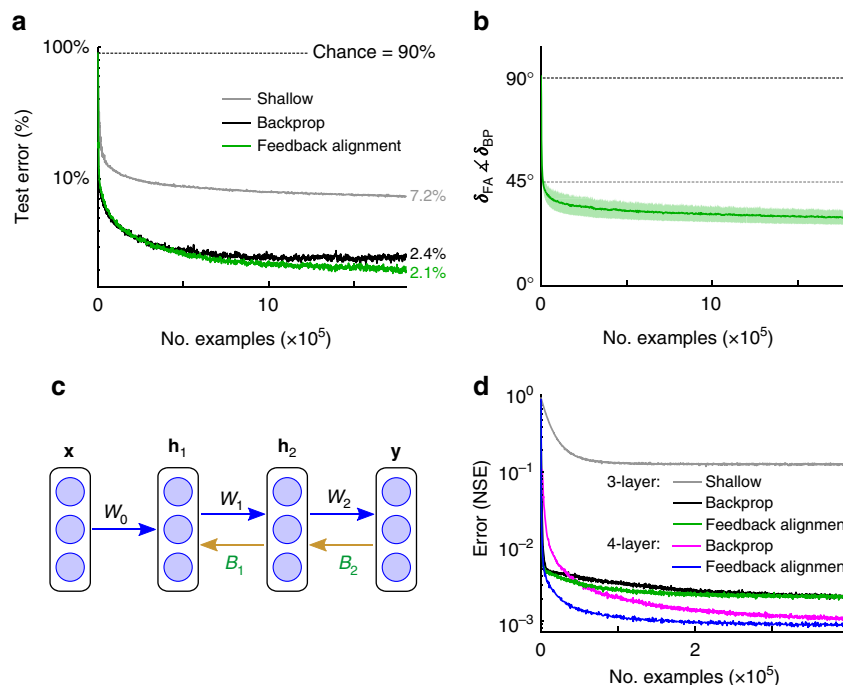


Figure 3 | Feedback alignment works in multilayer networks comprised of nonlinear neurons. (a) A 784-1000-10 network of logistic units learns to recognize handwritten digits. Curves show performance by backprop (black), feedback alignment (green) and shallow learning (grey) on 10,000 test images. (b) In the nonlinear case shown in a, the modulator vectors prescribed by feedback alignment and backprop also align. Error bars are one s.d. around the time-averaged mean. (c) Feedback alignment can train deep networks. (d) Error curves for a nonlinear function-approximation task, for a three-layer network trained with shallow learning (grey), backprop (black) or feedback alignment (green), and for a four-layer network trained with backprop (magenta) or feedback alignment (blue).

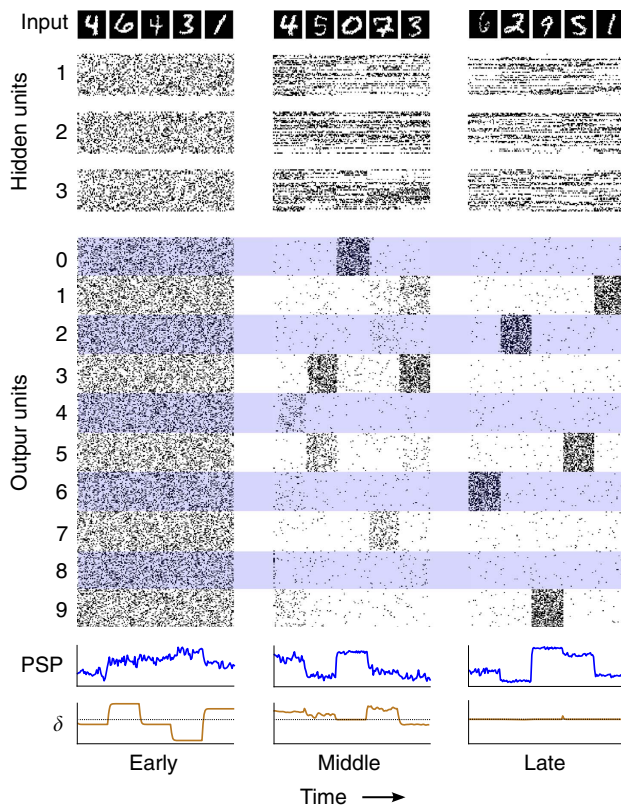


Figure 4 | Feedback alignment operates in larger networks with more complex dynamics. A network (784-1500-1500-1500-1000) of neurons that integrate their activity over time and spike stochastically, learns to recognize handwritten digits. The inputs (images along top) were presented to the network for 50 time steps each. Rasters show spikes of 50 randomly selected units from each of the three hidden layers (1, 2 and 3) and of the 1,000 output units (100 for each of the 10 classes, '0' through '9'). The plots at the bottom show that a single forward neuron's PSP and its modulatory signal δ_j (a.u.), evolve continuously and simultaneously. All variables are shown at three stages of learning: early; middle; and late.

MNIST data set, but this time in a network with three hidden layers, each comprised of 1,500 stochastic binary units whose integration window for synaptic inputs had a time constant of 0.9 (Fig. 4; see Methods). This network uses feedback alignment to learn to effectively classify handwritten digits (1.8% final error on the test set). To highlight the changes in network dynamics over the course of learning, we plotted a post-synaptic potential (PSP) of a forward neuron and that same neuron's modulatory signal, which is driven by the feedback δ_j (Fig. 4). Both variables evolve simultaneously, with no pauses or alternation, and the modulatory signal sculpts ongoing plasticity in a manner that depends on the pre- and post-synaptic activity of the neuron. The model incorporates only a small subset of the complexities found in real neural circuits; for example, it does not incorporate fixed spike thresholds or refractory periods. Nevertheless, it demonstrates that feedback alignment is still robust and able to implicitly adapt to random feedback in a more complex setting, where the forward and backward pathways both operate continuously. Therefore, the fact that feedback alignment relaxes the constraints on the connectivity patterns required for effective error propagation is evident even in more complex settings. The new mechanism also works to train deeper and wider networks, and on more difficult tasks, such as the Google SVHN data set (Supplementary Notes 2–9 and Supplementary Figs 7 and 8).

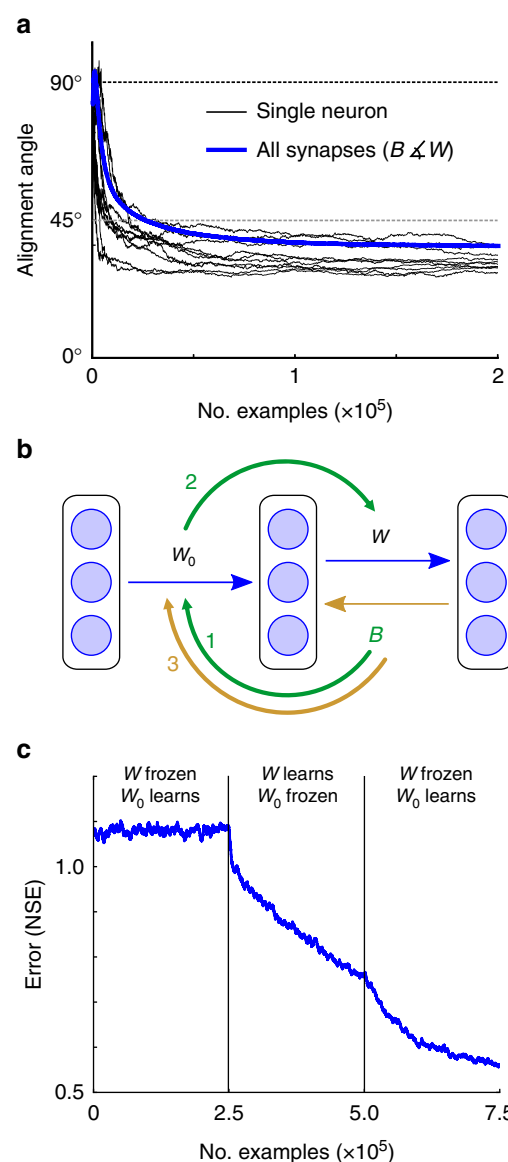


Figure 5 | Mechanics of feedback alignment. **(a)** W aligns with B^T (blue line), and single hidden neurons (black lines) exhibit the same alignment of their forward and feedback weights. **(b)** Schematic showing the information flow in feedback alignment. Synaptic weight information from B flows back into W_0 (1) and then forward into W (2). As W aligns with B^T , B begins to act like W^T , sending useful teaching signals to the hidden units (3). **(c)** To reveal this flow of information, we can artificially break the learning into three phases. In the first phase W is frozen while W_0 learns; this learning does not reduce the error because changes are driven by a feedback matrix B that is not aligned with W^T . In the second phase W_0 is frozen while W learns. In the third phase W is again frozen while W_0 learns, but now learning does reduce the error, because W aligned with B^T during phase 2.

Insight into the mechanics of feedback alignment. For insight into how feedback alignment operates, we returned to the observation that the modulator signals prescribed by feedback alignment come to resemble those prescribed by backprop (Figs 2 and 3). This process is central to feedback alignment's effectiveness and it occurs because the weight matrices in the forward pathway evolve to align with those in the feedback pathway (Fig. 5a and Supplementary Fig. 9). But why do they evolve this way? Under certain conditions it is possible to prove that feedback alignment will lead to the convergence of error to a

minimum, although these formal results provide limited intuition into how feedback alignment works (Supplementary Notes 10–16 and Supplementary Figs 10–14). We gained more insight about how the algorithm functions from some simple observations. To begin, note that while B and W do not directly communicate, it is still possible for B to influence the development of W in the course of learning (Fig. 5a). From equation (1), we have $\Delta W_0 \propto Bx^T$, which means that information about B accumulates in W_0 . This information then passes into W by its own learning rule, $\Delta W \propto \mathbf{e}\mathbf{h}^T = \mathbf{e}\mathbf{x}^TW_0^T$. In short, information about B flows into W_0 , altering W_0 so that it pushes W into alignment with B^T (Fig. 5b).

This process becomes visible when we artificially break the learning into phases (Fig. 5c), wherein: (1) W_0 is adjusted while W is kept frozen; (2) W is adjusted while W_0 is kept frozen; and (3) W_0 is once again adjusted, with W kept frozen. After information in B has travelled via W_0 into W in the first two phases, learning in the hidden layer now becomes effective, driven by errors propagated through B (Fig. 5c). It is possible to develop a more detailed argument for these intuitions and why W tends to align with B^T (Supplementary Notes 12 and Supplementary Figs 11 and 12). Indeed, additional experiments and analytic results suggested that feedback alignment may actually encourage W to align with the Moore-Penrose pseudoinverse of B (Supplementary Notes 13 and 14 and Supplementary Fig. 13)—a matrix that can be shown to be at least as useful as the transpose for conveying error (Supplementary Note 15). Taken together, whilst these observations do not provide a full account of how feedback alignment operates, they support the central implications for architectural constraints. What is crucial for effective error transmission is approximate functional symmetry. That is, B only needs to act like W^T , and feedback alignment demonstrates that this requirement is almost trivial to meet.

Discussion

The most effective forms of learning in large networks of neurons rely on mechanisms that adjust synaptic weights according to errors that are detected further downstream^{14,39}. In re-examining the conditions under which neural networks can exhibit such forms of deep learning, we have identified a new algorithm that we call feedback alignment. We show that in its simplest form, feedback alignment is able to make use of fixed, random connectivity patterns to update synaptic weights throughout a network. To our surprise, even with such minimal constraints on connectivity patterns, feedback alignment can achieve learning performances that are comparable to the backpropagation of error algorithm. Critically, this demonstrates that the kind of precise symmetric connectivity between layers of neurons that is required by backprop, is not essential to achieve effective transmission of errors across layers. In characterizing the performance of feedback alignment, we first demonstrated that the algorithm is effective in using error signals to update synaptic weights in simple linear and nonlinear networks. We then showed that feedback alignment is also effective in larger networks that incorporate multiple hidden layers and in networks that exhibit sparse connectivity or impose more realistic constraints on how activity is represented. Finally, our investigations into how feedback alignment works suggest that the algorithm's power relies on the fact that the weight matrices of the forward going synapses evolve to align approximately with those in the feedback pathway. Taken together, our study reveals much lower architectural constraints on what is required for error propagation across layers of neurons and thus provides insights into how neural circuits might support fast learning in large deep networks.

Feedback alignment offers a surprising and simple solution to the problem of synaptic 'weight transport'. As with many forms of learning that have been proposed to occur in the brain, it makes use of the idea that teaching signals could be carried by reciprocal connections^{7,21,24,25,29,40}. However, in the case of feedback alignment we have shown that this does not depend on detailed symmetric reciprocal connectivity, and yet it is still able to train large networks quickly. There are, of course, many outstanding questions regarding how the brain could utilize learning processes that rely on error propagation to adapt upstream synaptic connections in a network^{21,22}. This includes how exactly the brain computes and represents errors, and how the feedforward and feedback pathways might interact with one another. These issues are relevant for understanding any form of supervised learning and are not unique to the algorithm we describe. Nevertheless, these questions are important when considering the potential biological context for feedback alignment or future, related algorithms. In terms of error, an important question has been where the brain obtains labelled data for training a supervised system. A key insight has been that rather than requiring an external teacher, errors can result from mismatches between expected and actual perceptions, or between intended and realized motor consequences^{4,30,40}. For example, it is possible to derive teaching signals from sensory input by trying to predict one modality from another, by trying to predict the next term in a temporal sequence^{40,41} or by trying to encode and reconstruct sensory information^{42,43}. These processes can be thought of as supervised tasks, with the sensory activity itself playing the role of the teacher^{7,40,43,44}. Indeed, experimental data from a range of systems have shown that neuronal populations represent prediction mismatch and motor errors in their activity^{1–3,5–8,45–48}.

As with other forms of hierarchical learning, an important question is how feedforward and feedback pathways interact with one another in the brain. It is well established that there are extensive feedback pathways that carry information from 'higher' areas to 'lower' sensory areas and these connections have been shown to modulate the tuning properties and therefore the activity of neurons in lower areas^{49,50}. It therefore seems likely (perhaps inevitable) that this top-down modulation of neuronal activity will impact the learning that goes on in the lower area neuron's synapses. Indeed, recent work has demonstrated that learning in sensorimotor tasks alters representations in earlier cortical areas⁵¹. For higher layers to deliver error information that could enable lower layers to make useful changes to their synaptic weights, neurons in the lower layers should, at least in part, be able to differentiate a top-down error signal from activity originating in the forward pathway. Thus, a prediction is that one of the functions of the backward pathway is to ultimately modulate plasticity processes at the synapses of a neuron in the forward pathway. In this regard, it is interesting that experimental evidence has shown that various 'third-factors' can modulate the magnitude and sign of synaptic plasticity mechanisms. Depolarizing inputs arriving at specific times and/or subcellular compartments^{33–35}, neuromodulators^{52,53} and different types of synapse^{37,38} can all regulate plasticity resulting from the pairing of pre- and post-synaptic activity. For example, Sjöström *et al.*³³ demonstrated that Hebbian learning protocols that result in long-term potentiation at neocortical synapses can be altered to result in long-term depression if they occur simultaneously with local, subthreshold depolarizing inputs into the post-synaptic dendrite^{33,35}. And more recently, an empirically grounded learning mechanism has been proposed in which forward and teaching signals are delivered concurrently into dendritic and somatic compartments, respectively³⁶.

These observations suggest that there are a variety of plasticity mechanisms that would enable feedforward and feedback pathways to interact during learning. Indeed, any task-driven learning will require mechanisms that serve to modulate ongoing plasticity. Reinforcement learning, for example, requires the delivery of a global signal that can be thought of as a widespread third factor for regulating ongoing synaptic plasticity^{10,11}. At the other end of the spectrum, a learning algorithm such as backprop would require a much more highly orchestrated computation and delivery of third factors to individual neurons in the hidden layer. By contrast, feedback alignment represents a surprising middle ground, in that it has many of the performance advantages of backprop, but it markedly reduces the complexity of the machinery for computing and delivering third factors: the modulatory signals in feedback alignment can be delivered via random connections by one or many neurons in the backward pathway, to one or many neurons in hidden layers, and the modulatory signals are themselves computed on the basis of random connections in the backward pathway.

Nevertheless, there remains many questions about how the brain uses error signals that are passed across multiple layers of neurons. For example, in our simplified models (for example, Fig. 2), error signals modulate the synaptic strengths of feedforward connections without affecting the post-synaptic activities. Whilst various third factors could play a role in delivering error signals without significantly altering activity in the forward path (see above), it seems more likely that feedback in real neuronal circuits will influence the post-synaptic activity in lower layers. Feedback alignment uses top-down connections to make small and gradual adjustments to the synaptic weights so that future data are processed in a more optimal manner. On a much faster timescale however, the same top-down connections are likely to be important for improving inference on the current inputs (that is, hidden variable estimation). A challenge for future work therefore, is to understand how top-down connections can be used to simultaneously support inference and learning^{15,40}. A related question for the field is how error signals from higher layers can be integrated with bottom-up, unsupervised learning rules^{43,54}.

A key insight from machine learning work is that the most powerful learning algorithms use some form of error propagation for gradient estimation, and that without gradient-based algorithms such as backprop, learning remains intractably slow for difficult problems. Recent advances in supervised learning have achieved state-of-the-art and even human-level performance by training deep networks on large data sets by applying variants of the backprop algorithm^{55,56}. The most effective forms of reinforcement and unsupervised learning also rely on the ability to transmit detailed error information across multiple layers of neurons^{15,16}. Recently, reinforcement learning has been used to achieve impressive results using simple temporal-difference error signals, but these results hinge crucially on backpropagation. These reinforcement signals are not delivered as a global modulatory signal, but are carefully backpropagated through the deep network that supports behaviour¹⁶. Unsupervised learning algorithms that obtain state-of-the-art results also rely on backprop, such as variational auto-encoders and networks that predict perceptual information in a sequence^{15,17}.

Whilst theoretical, these advances in machine learning provide a context in which to examine different learning processes in the brain. In particular, they strengthen the case for looking beyond naive learning rules that broadcast the same global scalar summary of error to every neuron. Such rules are, on their own, likely too slow for training very large deep networks to perform difficult tasks. In this context it is again useful to think of feedback alignment as one of many algorithms that lie on a

'spectrum' between naive global updates and precise gradient-based updates. An interesting point on this spectrum is work showing that reinforcement learning on binary decision tasks can be sped up if, in addition to a global scalar reward, each neuron also receives information about the population decision¹¹. An earlier study examined using asymmetric weights in the context of simple classification tasks solved via attention-gated reinforcement learning³², although this approach still made use of a global scalar reward. Moving a little closer to backprop, feedback alignment is extremely simple and makes few demands on connectivity, and yet it quickly learns to deliver useful estimates of the gradient tailored to individual neurons. Indeed, it is reasonable to suppose that there is a large family of algorithms that the brain might exploit to speed up learning by passing expectation or error information between layers of neurons. Although we have found that random feedback connections are remarkably good at conveying detailed error signals, we anticipate future algorithms that will better capture the details of neural circuits and incorporate different mechanisms for delivering effective teaching signals. Indeed, recent work presents further evidence that weight symmetry is not crucial for effective error propagation⁵⁷ (Supplementary Notes 2–9). These experiments highlight the importance of the signs of the delivered gradients and that error propagation via asymmetric connections can be improved by techniques such as batch normalization⁵⁸.

Our results also hint that more complex algorithms could benefit from the implicit dynamics inherent in feedback alignment, which naturally drive forward synapses into alignment with the backward matrices. For example, these dynamics may work well with architectures or circuits in which B is adjusted as well as W , to further encourage functional alignment between W and B (perhaps by training the backward weights to reproduce the activity of the layer below, as in layer-wise autoencoder training with untied weights). Finally, deep learning innovations may provide insight into other questions that have surrounded the implementation of learning in the brain. For example, while backprop is usually applied in artificial networks that transmit information using continuous rather than discrete stochastic values, recent developments in machine learning suggest roles for 'spiking' activities. Not only can backprop-like mechanisms work well in the context of discrete stochastic variables⁵⁹, random transmission of activities also forms the basis of powerful regularization schemes like 'dropout'⁵⁶. These recent insights into learning in large, multi-layer networks provide a rich context for further exploring the potential for feedback alignment and related algorithms, which may help explain fast and powerful learning mechanisms in the brain.

The issue of how the brain might propagate detailed error signals from one region to another is a fundamental question in neuroscience. Recent theories of brain function have suggested that cortex uses hierarchical message passing wherein both predictions and prediction errors are communicated between layers, or areas, of cortex^{40,44}. And recent experimental work has shown that high-level visual response properties in cortex are significantly better explained by models that are optimized by transmitting errors back across many layers of neurons⁶⁰, than by models that are trained via layer-wise unsupervised learning. In the 1980s, new learning algorithms promised to provide insight into brain function^{14,21}. But the most powerful of these (that is, learning by backpropagation of error) has seemed difficult to imagine implementing in the brain^{21,22}. There are a number of questions about how neural circuits might implement error propagation, but one of the most central and enduring issues concerns the constraints on connectivity patterns between layers—that is, because backprop requires weight transport to tailor error signals for each neuron in a network^{21,22,24}. Our

observations and experimental results dispel the central assumptions implicit in the statement of the weight transport problem. Instead, we demonstrate that the constraints on the connectivity required to support effective error transport are much less demanding than previously supposed. Starting with random feedback, standard update rules quickly push the forward pathway into a soft alignment with the fixed feedback pathway, allowing relevant error information to flow. Taken together with recent theoretical and empirical advances, our work supports revisiting the idea of backprop-like learning in the brain and may provide insights into how neural circuits could implement fast learning in large deep networks.

Methods

Summary. In the simulations in Fig. 2, a 30-20-10 linear network was trained by backprop, feedback alignment or a fast form of reinforcement learning called node perturbation^{12,61}. All algorithms trained on the same sequence of input/output pairs, with $\mathbf{x} \sim \mathcal{N}(\mu = 0, \Sigma = I)$, $\mathbf{y}^* = T\mathbf{x}$. The larger, nonlinear networks in Figs 3a,b and 4 were trained with 60,000 images from the MNIST data set, and tested on a held-aside set of 10,000 images. In Fig. 3d, a 30-20-10 and a 30-20-10-10 network learned to approximate the output of a 30-20-10-10 target network, using backprop or feedback alignment. All three networks had tanh(\cdot) hidden units and linear output units. Both algorithms were trained on the same examples, with $\mathbf{x} \sim \mathcal{N}(\mu = 0, \Sigma = I)$, $\mathbf{y}^* = W_2 \tanh(W_1 \tanh(W_0 \mathbf{x} + \mathbf{b}_0) + \mathbf{b}_1) + \mathbf{b}_2$. In Fig. 5, a 20-1000-20 network with tanh(\cdot) hidden units and linear output units learned to match a quadratic target function. Comparing the performance of different learning algorithms is notoriously tricky^{39,62}. To keep things simple and avoid favouring our own method, we used fixed learning rates and chose hyperparameters to optimize backprop, as described below. An earlier version of this work appeared on arXiv.org⁶³.

Linear function approximation. In the networks of Fig. 2a,b the target linear function T mapped vectors from a 30- to a 10-dimensional space. The elements of T were drawn at random, that is, uniformly from the range $[-1, 1]$. Once chosen, the target matrix was fixed, so that each algorithm tried to learn the same function. Output weights were adjusted via $\Delta W \propto \mathbf{e}\mathbf{h}^T$ for all three algorithms. Hidden weights were adjusted according to (a) backprop, $\Delta W_0 \propto \delta_{BP}\mathbf{x}^T$, where $\delta_{BP} = W^T\mathbf{e}$; (b) feedback alignment, $\Delta W_0 \propto \delta_{FA}\mathbf{x}^T$, where $\delta_{FA} = \mathbf{B}\mathbf{e}$ with the elements of B drawn from the uniform distribution over $[-0.5, 0.5]$; or (c) a fast variant of reinforcement learning called node perturbation^{12,61}. We chose the learning rate η for each algorithm via manual search⁶⁴ to optimize learning speed. The elements of the network weight matrices, W_0 and W , were initialized by drawing uniformly from the range $[-0.01, 0.01]$. For node perturbation reinforcement learning, we optimized the scale of the perturbation variance^{12,61} by manual search⁶⁴.

Nonlinear networks. In the nonlinear networks of Figs 3a,d,4 and 5a,c, synaptic change depended on the post-synaptic cell's activity. For instance, a hidden unit with output h_j and sigmoid nonlinearity will update its incoming synaptic weights by the three-factor formula $\Delta W_0^{ij} = \delta_j x_i [h_j(1 - h_j)]$. Here the term $h_j(1 - h_j)$ enters because it is the derivative of the cell's sigmoid nonlinearity. Similarly, a hidden unit with output h_j and tanh(\cdot) nonlinearity will update its incoming synaptic weights by the formula $\Delta W_0^{ij} = \delta_j x_i (1 - h_j^2)$. Importantly, these derivatives are used only locally: with feedback alignment, there is no need to transmit the derivatives between cells or layers; all that is needed is that each cell's synaptic adjustments depend on its own activity, in this case h_j . Urbanczik and Senn³⁶ have proposed a related three-factor learning rule and we note that such derivatives are simple positive functions of the post-synaptic cell's activity—that is, the post-synaptic dependence differs from 'pure' Hebbian learning only in that it prescribes smaller updates at the extremes of the cell's activity. In practice, we have found that rough approximations of this weighting function work nearly as well as the exact version.

MNIST data set. For both backprop and feedback alignment in Fig. 3a,b, the output weights were adjusted via $\Delta W \propto (\mathbf{e} \circ \mathbf{y}')\mathbf{h}^T$. Hidden weights were adjusted according to (a) backprop: $\Delta W_0 \propto (\delta_{BP} \circ \mathbf{h}')\mathbf{x}^T$, where $\delta_{BP} = W^T(\mathbf{e} \circ \mathbf{y}')$; (b) feedback alignment: $\Delta W_0 \propto (\delta_{FA} \circ \mathbf{h}')\mathbf{x}^T$, where $\delta_{FA} = \mathbf{B}\mathbf{e}$. Here \circ is element-wise multiplication and \mathbf{y}' and \mathbf{h}' are the derivatives of the output unit and hidden unit activations, respectively. We manually optimized the learning parameters to give good performance with the backprop algorithm. That is, the elements of W_0 and W were drawn from the uniform distribution over $[-\omega, \omega]$, where ω was selected by looking at final performance on the test set. We used the standard training and test sets⁶⁵ and desired outputs were coded using standard 1-hot representations. We used a learning rate of, $\eta = 10^{-3}$, and weight decay constant of, $\alpha = 10^{-6}$. The same learning parameters were used with feedback alignment. The elements of the B matrix were drawn from a uniform distribution over $[-\beta, \beta]$ with β chosen by manual search. Empirically, we found that many scale parameters for B worked well. In practice it required five restarts to select the scale used for B in the

simulations presented here. Once a scale for B was chosen, a new B matrix was drawn for each of the $n=20$ simulations. In the experiments where 50% of the weights in W and B were removed, we drew the remaining elements from the same uniform distributions as above (that is, using ω and β). Learning was terminated after the same number of iterations for each simulation and for each algorithm. We selected the termination time by observing when backprop began to overfit on the test set.

Deep nonlinear function approximation. In Fig. 3d the weights for the target network, $T(\cdot)$, were chosen at random from a uniform distribution and then fixed for the corresponding simulations. The output unit updates for both backprop and feedback alignment were adjusted via $\Delta W_2 \propto (\mathbf{e} \circ \mathbf{y}')\mathbf{h}_1^T$. Hidden unit updates were adjusted according to (a) backprop: $\Delta W_1 \propto (\delta_2 \circ \mathbf{h}_2')\mathbf{h}_1^T$, where $\delta_2 = W_2^T(\mathbf{e} \circ \mathbf{y}')$, and $\Delta W_0 \propto (\delta_1 \circ \mathbf{h}_1')\mathbf{x}^T$ with $\delta_1 = W_1^T(\delta_2 \circ \mathbf{h}_2')$ for the deeper hidden layer. (b) Feedback alignment: $\Delta W_1 \propto (\delta_2 \circ \mathbf{h}_2')\mathbf{h}_1^T$, where $\delta_2 = B_2\mathbf{e}$, and $\Delta W_0 \propto (\delta_1 \circ \mathbf{h}_1')\mathbf{x}^T$ with $\delta_1 = B_1\delta_2$ for the deeper hidden layer. We chose a range $(-\alpha, \alpha)$ with $\alpha = 0.5$ for the uniform distribution from which weights were drawn for the target network; in this case backprop gained an unambiguous advantage from having an additional hidden layer. A new set of random forward weights and biases and feedback weights were chosen for each of the $n=20$ simulations. The elements of B_1 and B_2 were also drawn from a uniform distribution and fixed across simulations. Learning was terminated after the same number of iterations for each simulation and for each algorithm.

Quadratic function approximation. In Fig. 5a,c, training pairs were produced by $y_k^* = \mathbf{x}^T Q_k \mathbf{x}$, for $k \in \{1, \dots, 20\}$, with the elements of \mathbf{x} chosen from a uniform distribution over $[-2, 2]$. The parameters for the quadratic target function, that is, the elements of each Q_k , were chosen uniformly at random from the interval $[-0.5, 0.5]$. The initial weights and biases, and the elements of the feedback matrix, were drawn from the uniform distributions with manually selected scale parameters. Unit updates were as described in the methods for Fig. 3a,b.

Angle measures. Throughout, the angle between two vectors, for example, $\mathbf{a} \wedge \mathbf{b}$, was computed as $\theta = \cos^{-1}(\|\mathbf{a}^T \mathbf{b}\| / (\|\mathbf{a}\| \cdot \|\mathbf{b}\|))$. When speaking of the angle between two matrices, we simply 'flatten' the matrices into vectors. In Fig. 5a, we examined the angle between the forward and backward paths for randomly sampled hidden units. That is, for the j th hidden unit, we measured the angle between the outgoing forward weights given by the j th column of W , and incoming feedback weights given by the j th row of B .

Normalized squared error. We used a normalized squared error measure for regression problems where the units of error are not particularly meaningful. The loss for each model, in this case the sum of squared errors, was normalized by the sum of the squared error that one would achieve if using the sample mean as the model. This is the natural, albeit uncommon, normalization term for the sum of squared errors loss. The normalization term is thus

$$1/T \sum_t \sum_i (y_i(t) - \bar{y}_i)^2 \quad (2)$$

$$= 1/T \sum_t \sum_i (y_i(t))^2 - 2\bar{y}_i * y_i(t) + \bar{y}_i^2 \quad (3)$$

$$= 1/T \sum_t \sum_i (y_i(t))^2 - \bar{y}_i^2 \quad (4)$$

Here t indexes the batch, T is the length of the batch and i indexes the dimensions of the output. This measure generates learning curves that are almost always contained within the range $[0, 1]$, except in the case that a model 'blows up' and has worse error than when the learning is started.

A deep network that integrates its activity and spikes. As a proof of principle that feedback alignment can operate in a simple network architecture where forward and backward dynamics are simultaneous, we constructed a network of neurons that continuously integrate their activity (Fig. 4). In designing this model, we aimed for a level of detail that conveyed this essential point, while remaining simple enough to allow large-scale simulations. The consideration of scalability was particularly relevant as we aimed to demonstrate efficacy in a real-world learning task. The dynamics of the neural activities and synaptic plasticity operate simultaneously, but for clarity we describe them separately. Network and plasticity dynamics are similar in some respects to those developed by Urbanczik and Senn³⁶. The architecture and operation of the network are diagrammed in the Supplementary Information (Supplementary Figs 3 and 4).

Neurons in the forward path have the following activity dynamics: the PSP of a hidden neuron j in layer l , V_j^l , at time t was modelled as

$$V_j^l(t) = [1 - \tau] V_j^l(t-1) + \tau \sum_i W^{ij}(t) \phi_h(V_i^{l-1}(t)). \quad (5)$$

Here τ is the integration time constant; ϕ_h is the binary spiking activity of the hidden neurons, i , in the preceding layer, $l-1$; and $W^{ij}(t)$ is the synaptic strength

from neurons h_i^{l-1} to h_j^l . The spiking activity, ϕ_h , of neuron h_j^l at time t is a Bernoulli random variable determined by a sigmoidal function of its potential; the neuron spikes, that is, $\phi_h(V_j^l(t)) = 1$, with probability $1/(1 + \exp(-V_j^l(t)))$, and 0 otherwise.

During learning an MNIST image, $\mathbf{x}(t)$ was presented to the network for $N=5$ consecutive time steps before switching to the next image in the training set. Notably, there was no interruption of the neural activity or plasticity dynamics during this switch. We interpreted MNIST pixel values (normalized to between 0 and 1) as probabilities of spiking in the input layer of the network. The probability of a given input neuron spiking was computed directly from the image and saturated at 0.95. That is, a neuron in the input layer spiked, $\phi_h(x_j(t)) = 1$, with probability $\min[x_j(t), 0.95]$. Thus, inputs to the network varied from time step to time step.

Neurons in the backward pass had similar dynamics. The PSP of a feedback neuron j in layer l , U_j^l , at time t was modelled as

$$U_j^l(t) = [1 - \tau]U_j^l(t-1) + \tau \sum_k B_{jk}^l \phi_\delta(U_k^{l+1}(t)). \quad (6)$$

Again τ is the integration time constant. Here ϕ_δ is a simple sigmoidal function centred on 0, and B_{jk}^l is the synaptic strength from neurons h_k^{l+1} to h_j^l . Thus, the backward neurons function similarly to climbing fibres in the cerebellum, which are tonically active, allowing encoding of negative errors: an increase in climbing fibre firing rate drives LTD at parallel-fibre inputs to Purkinje cells, and a decrease drives LTP^{37,38}.

The potential of a feedback neuron δ_j^m in the final layer m , which can be thought of as an error neuron, was:

$$U_j^m(t) = [1 - \tau]U_j^m(t-1) + \tau(\phi_h(V_j^m(t)) - \phi_j^*(t)). \quad (7)$$

We used 1,000 output neurons, with 100 neurons associated with each output class ('0'-'9'). Thus, we set $\phi_j^*(t) = 1$ if output neuron h_j^m was associated with the class currently being presented to the network, and $\phi_j^*(t) = 0$ otherwise.

The plasticity at the forward synapses, $W_{ij}^l(t)$, is ongoing. That is, synaptic plasticity occurs at every time step and is a function of three factors: (i) the pre-synaptic activity, $\phi_h(V_i^{l-1}(t))$; (ii) the post-synaptic activities, $\phi_h(V_j^l(t))$; and (iii) a modulatory third factor delivered by neurons in the feedback path, $\phi_\delta(U_j^l(t))$:

$$\Delta W_{ij}^l(t) \propto \phi_\delta(U_j^l(t)) \cdot \phi_h(V_i^{l-1}(t)) \cdot \Psi_h(V_j^l(t)). \quad (8)$$

Where, $\Psi_h(\cdot)$ is a simple positive weighting function of the post-synaptic voltage—the derivative of the logistic function, which is used only local to the post-synaptic neuron. Urbanczik and Senn³⁶ have suggested a related three-factor learning rule, and our pre- and post-synaptic terms are analogous. But in their model, desired outputs are delivered to the somatic compartment and the error term is computed locally by a neuron as the difference between somatic spiking and a prediction made by the dendritic compartment.

The dynamics during testing were identical except that synaptic plasticity was arrested. Performance was evaluated as the number of correct guesses on the standard test set. A guess was generated by choosing the output class with highest activity, that is, the $\phi_h(V_j^m(t))$ summed over the groups of neurons associated with each output class, after $M=5$ time steps of exposure to a test image. The forward and backward matrices were initialized randomly by drawing from the uniform distribution over $[-0.05, 0.05]$ and $[-0.1, 0.1]$, respectively. We used a fast time constant of $\tau=0.9$ to permit quick simulation of the model during training. We used a standard weight decay term of $\gamma=10^{-8}$ for all forward weights and biases, and a constant learning rate of $\eta=10^{-3}$.

Programming. All learning experiments were run using custom built code in Python with the Numpy library. MNIST experiments were sped up using a GPU card with the Cudamat and Gnumpy libraries^{66,67}.

Data availability. The data sets used by this study are publicly available. Code is available from the corresponding authors on request.

References

- Bell, C., Bodznick, D., Montgomery, J. & Bastian, J. The generation and subtraction of sensory expectations within cerebellum-like structures. *Brain Behav. Evol.* **50**, 17–31 (1997).
- Kitazawa, S., Kimura, T. & Yin, P.-B. Cerebellar complex spikes encode both destinations and errors in arm movements. *Nature* **392**, 494–497 (1998).
- Schultz, W. & Dickinson, A. Neuronal coding of prediction errors. *Annu. Rev. Neurosci.* **23**, 473–500 (2000).
- Hinton, G. The ups and downs of Hebb synapses. *Can. Psychol.* **44**, 10–13 (2003).
- Keller, G. B. & Hahnloser, R. H. Neural processing of auditory feedback during vocal practice in a songbird. *Nature* **457**, 187–190 (2009).
- Keller, G. B., Bonhoeffer, T. & Hubener, M. Sensorimotor mismatch signals in primary visual cortex of the behaving mouse. *Neuron* **74**, 809–815 (2012).
- Bastos, A. M. et al. Canonical microcircuits for predictive coding. *Neuron* **76**, 695–711 (2012).
- Ito, M. Error detection and representation in the olivo-cerebellar system. *Front. Neural Circuits* **7**, 1 (2013).
- Mazzoni, P., Anderson, R. A. & Jordan, M. I. A more biologically plausible learning rule for neural networks. *Proc. Natl Acad. Sci. USA* **88**, 4433–4437 (1991).
- Seung, H. S. Learning in spiking neural networks by reinforcement of stochastic synaptic transmission. *Neuron* **40**, 1063–1073 (2003).
- Urbanczik, R. & Senn, W. Reinforcement learning in populations of spiking neurons. *Nat. Neurosci.* **12**, 250–252 (2009).
- Werfel, J., Xie, X. & Seung, H. S. Learning curves for stochastic gradient descent in linear feedforward networks. *Neural Comput.* **17**, 2699–2718 (2005).
- Saxe, A. M., McClelland, J. L. & Ganguli, S. Exact solutions to the nonlinear dynamics of learning in deep linear neural networks. Preprint at <https://arxiv.org/abs/1312.6120> (2013).
- Rumelhart, D. E., Hinton, G. E. & Williams, R. J. Learning representations by back-propagating errors. *Nature* **323**, 533–536 (1986).
- Kingma, D. P. & Welling, M. Auto-encoding variational bayes. Preprint at <https://arxiv.org/abs/1312.6114> (2013).
- Mnih, V. et al. Human-level control through deep reinforcement learning. *Nature* **518**, 529–533 (2015).
- Srivastava, N., Mansimov, E. & Salakhutdinov, R. Unsupervised learning of video representations using LSTMs. Preprint at <https://arxiv.org/abs/1502.04681> (2015).
- Zipser, D. & Andersen, R. A. A back-propagation programmed network that simulates response properties of a subset of posterior parietal neurons. *Nature* **331**, 679–684 (1988).
- Lillicrap, T. P. & Scott, S. H. Preference distributions of primary motor cortex neurons reflect control solutions optimized for limb biomechanics. *Neuron* **77**, 168–179 (2013).
- Yamins, D. L. et al. Performance-optimized hierarchical models predict neural responses in higher visual cortex. *Proc. Natl Acad. Sci. USA* **111**, 8619–8624 (2014).
- Crick, F. The recent excitement about neural networks. *Nature* **337**, 129–132 (1989).
- Grossberg, S. Competitive learning: from interactive activation to adaptive resonance. *Cogn. Sci.* **11**, 23–63 (1987).
- Stork, D. G. in *International Joint Conference on Neural Networks*, Vol. II, 241–246 (Piscataway, 1989).
- Zipser, D. & Rumelhart, D. E. in *Computational Neuroscience*. (ed. Schwartz, E. L. Ch. 15) 192–200 (MIT Press, 1990).
- Kording, K. P. & König, P. Supervised and unsupervised learning with two sites of synaptic integration. *J. Comput. Neurosci.* **11**, 207–215 (2001).
- Harris, K. D. Stability of the fittest: organizing learning through retroaxonal signals. *Trends Neurosci.* **31**, 130–136 (2008).
- Abdelghani, M., Lillicrap, T. & Tweed, D. Sensitivity derivatives for flexible sensorimotor learning. *Neural Comput.* **20**, 2085–2111 (2008).
- Brandt, R. D. & Lin, F. in *Neural Networks*, 1996, IEEE International Conference on, Vol. 1, 300–305 (IEEE, 1996).
- Kolen, J. F. & Pollack, J. B. in *IEEE World Congress on Computational Intelligence*, Vol. 3, 1375–1380 (Orlando, 1994).
- O'Reilly, R. C. Biologically plausible error-driven learning using local activation differences: the generalized recirculation algorithm. *Neural Comput.* **8**, 895–938 (1996).
- Xie, X. & Seung, H. S. Equivalence of backpropagation and contrastive Hebbian learning in a layered network. *Neural Comput.* **15**, 441–454 (2003).
- Roelfsema, P. R. & Ooyen, A. v. Attention-gated reinforcement learning of internal representations for classification. *Neural Comput.* **17**, 2176–2214 (2005).
- Sjöstrom, P. J. & Häusser, M. A cooperative switch determines the sign of synaptic plasticity in distal dendrites of neocortical pyramidal neurons. *Neuron* **51**, 227–238 (2006).
- Kwag, J. & Paulsen, O. The timing of external input controls the sign of plasticity at local synapses. *Nat. Neurosci.* **12**, 1219–1221 (2009).
- Clopath, C. & Gerstner, W. Voltage and spike timing interact in STDP—a unified model. *Front. Synaptic Neurosci.* **2**, 25 (2010).
- Urbanczik, R. & Senn, W. Learning by the dendritic prediction of somatic spiking. *Neuron* **81**, 521–528 (2014).
- Coesmans, M., Weber, J. T., De Zeeuw, C. I. & Hansel, C. Bidirectional parallel fiber plasticity in the cerebellum under climbing fiber control. *Neuron* **44**, 691–700 (2004).
- Yang, Y. & Lisberger, S. G. Purkinje-cell plasticity and cerebellar motor learning are graded by complex-spike duration. *Nature* **510**, 529–532 (2014).
- Bengio, Y. & LeCun, Y. in *Large Scale Kernel Machines*. (eds Leon, B., Olivier, C., DeCoste, D. & Weston, J.) (MIT Press, 2007).
- Friston, K. The free-energy principle: a unified brain theory? *Nat. Rev. Neurosci.* **11**, 127–138 (2010).
- Elman, J. L. Finding structure in time. *Cogn. Sci.* **14**, 179–211 (1990).

42. Hinton, G. & McClelland, J. in *Neural Information Processing Systems*. (ed. Anderson, D.) 358–366, (1988).
43. Hinton, G., Osindero, S. & Teh, Y. A fast learning algorithm for deep belief nets. *Neural Comput.* **18**, 1527–1554 (2006).
44. Wacongne, C. *et al.* Evidence for a hierarchy of predictions and prediction errors in human cortex. *Proc. Natl Acad. Sci. USA* **108**, 20754–20759 (2011).
45. Eliades, S. J. & Wang, X. Neural substrates of vocalization feedback monitoring in primate auditory cortex. *Nature* **453**, 1102–1106 (2008).
46. Ahrens, M. B. *et al.* Brain-wide neuronal dynamics during motor adaptation in zebrafish. *Nature* **485**, 471–477 (2012).
47. Rao, R. P. & Ballard, D. H. Predictive coding in the visual cortex: a functional interpretation of some extra-classical receptive-field effects. *Nat. Neurosci.* **2**, 79–87 (1999).
48. Ito, M. Cerebellar long-term depression: characterization, signal transduction, and functional roles. *Physiol. Rev.* **81**, 1143–1196 (2001).
49. Gilbert, C. D. & Li, W. Top-down influences on visual processing. *Nat. Rev. Neurosci.* **14**, 350–363 (2013).
50. Zhang, S. *et al.* Long-range and local circuits for top-down modulation of visual cortex processing. *Science* **345**, 660–665 (2014).
51. Poort, J. *et al.* Learning enhances sensory and multiple non-sensory representations in primary visual cortex. *Neuron* **86**, 1478–1490 (2015).
52. Seol, G. H. *et al.* Neuromodulators control the polarity of spike-timing-dependent synaptic plasticity. *Neuron* **55**, 919–929 (2007).
53. Pawlak, V., Wickens, J. R., Kirkwood, A. & Kerr, J. N. Timing is not everything: neuromodulation opens the STDP gate. *Front. Synaptic Neurosci.* **2**, 146 (2010).
54. Clopath, C., Longtin, A. & Gerstner, W. An online hebbian learning rule that performs independent component analysis. *BMC Neurosci.* **9**, O13 (2008).
55. Ciresan, D., Meier, U., Gambardella, L. & Schmidhuber, J. Deep big simple neural nets for handwritten digit recognition. *Neural Comput.* **22**, 3207–3220 (2010).
56. Hinton, G. E., Srivastava, N., Krizhevsky, A., Sutskever, I. & Salakhutdinov, R. R. Improving neural networks by preventing co-adaptation of feature detectors. Preprint at <https://arxiv.org/abs/1207.0580> (2012).
57. Liao, Q., Leibo, J. Z. & Poggio, T. How important is weight symmetry in backpropagation? Preprint at <http://arxiv.org/abs/1510.05067> (2015).
58. Ioffe, S. & Szegedy, C. Batch normalization: accelerating deep network training by reducing internal covariate shift. Preprint at <https://arxiv.org/abs/1502.03167> (2015).
59. Soudry, D., Hubara, I. & Meir, R. in: *Advances in Neural Information Processing Systems*, 963–971 (2014).
60. Cadieu, C. F. *et al.* Deep neural networks rival the representation of primate it cortex for core visual object recognition. *PLoS Comput. Biol.* **10**, e1003963 (2014).
61. Williams, R. Simple statistical gradient-following algorithms for connectionist reinforcement learning. *Mach. Learn.* **8**, 229–256 (1992).
62. Wolpert, D. The lack of a priori distinction between learning algorithms. *Neural Comput.* **8**, 1341–1390 (1996).
63. Lillicrap, T. P., Cownden, D., Tweed, D. B. & Akerman, C. J. Random feedback weights support learning in deep neural networks. Preprint at <http://arxiv.org/abs/1411.0247> (2014).
64. Bergstra, J. & Bengio, Y. Random search for hyper-parameter optimization. *J. Mach. Learn. Res.* **13**, 281–305 (2012).
65. LeCun, Y., Bottou, L., Bengio, Y. & Haffner, P. in: *Proceedings of the IEEE*, Vol. 86, 2278–2324 (1998).
66. Mnih, V. *Cudamat: A Cuda-based Matrix Class for Python*. Technical Report UTML TR 2009-004 (University of Toronto, Ontario, Canada, 2009).
67. Tielemans, T. *Gnumpy: An Easy Way to Use GPU Boards in Python*. Technical Report UTML TR 2010-002 (University of Toronto, Toronto, Ontario, Canada, 2010).

Acknowledgements

We thank Geoffrey Hinton, Grzegorz Swirszcz and Ilya Sutskever for comments. The research leading to these results has received funding from the European Community's Seventh Framework Programme (FP7/2007–2013) under grant agreement number 632240, NSERC grant 391349–2010, and the Swedish Research Council 2009–2390.

Author contributions

T.P.L. and C.J.A. conceived the project; T.P.L., D.C. and D.B.T. ran the simulations; T.P.L., D.C., D.B.T. and C.J.A. wrote the Supplementary Information; T.P.L., D.C., D.B.T. and C.J.A. wrote the manuscript.

Additional information

Supplementary Information accompanies this paper at <http://www.nature.com/naturecommunications>

Competing financial interests: T.P.L., D.C., D.B.T. and C.J.A. have applied for a patent relating to the use of feedback alignment in training neural network systems (United States Patent and Trademark Office, serial number: 61/858,928). The remaining authors declare no competing financial interests.

Reprints and permission information is available online at <http://npg.nature.com/reprintsandpermissions/>

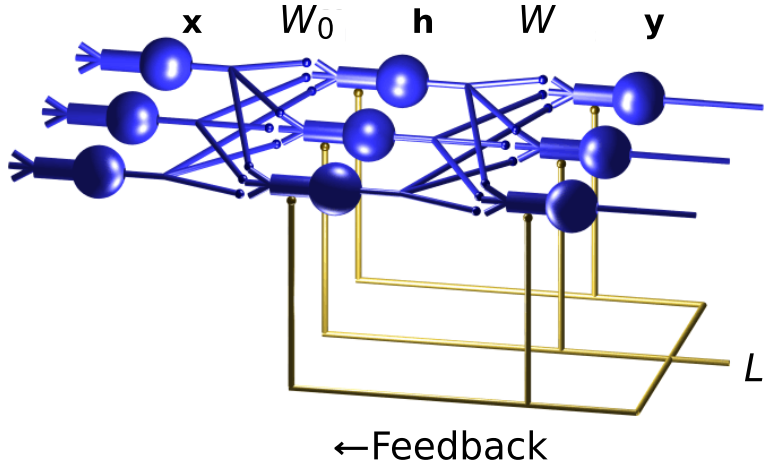
How to cite this article: Lillicrap, T. P. *et al.* Random synaptic feedback weights support error backpropagation for deep learning. *Nat. Commun.* **7**, 13276 doi: 10.1038/ncomms13276 (2016).

Publisher's note: Springer Nature remains neutral with regard to jurisdictional claims in published maps and institutional affiliations.

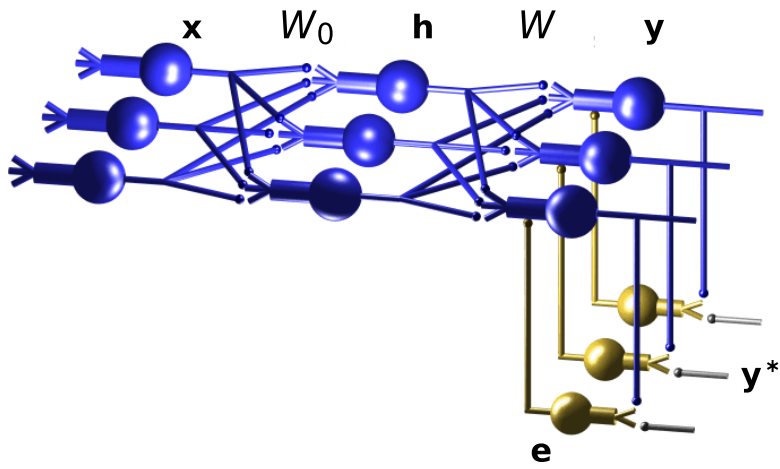


This work is licensed under a Creative Commons Attribution 4.0 International License. The images or other third party material in this article are included in the article's Creative Commons license, unless indicated otherwise in the credit line; if the material is not included under the Creative Commons license, users will need to obtain permission from the license holder to reproduce the material. To view a copy of this license, visit <http://creativecommons.org/licenses/by/4.0/>

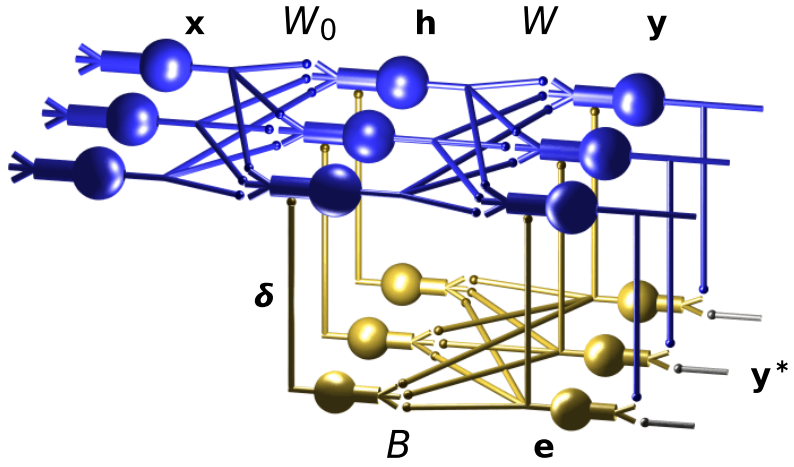
© The Author(s) 2016



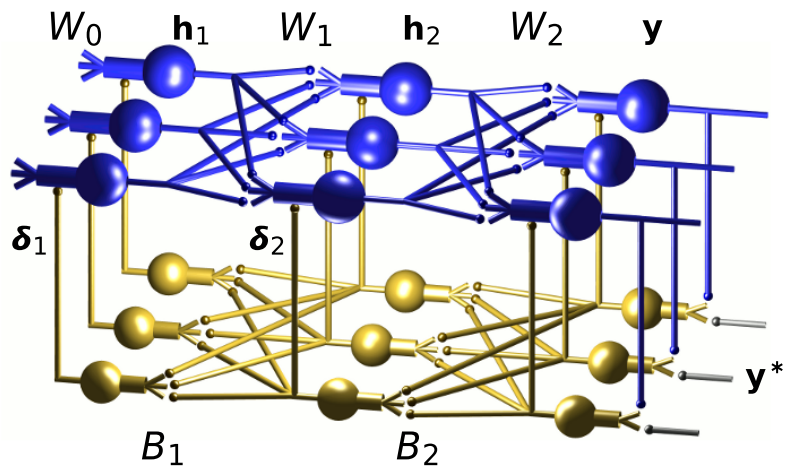
Supplementary Figure 1: Schematic of reinforcement learning in a multilayer network. The forward path is computed by the blue neurons at top. Input enters at the leftmost input neurons, x , and is transformed to hidden activity by, $\mathbf{h} = \phi(W_0\mathbf{x})$, where $\phi(\cdot)$ is the transfer function. Output via the rightmost neurons, y , is computed from the hidden neurons as, $\mathbf{y} = \phi(W\mathbf{h})$. An error, \mathbf{e} , between a desired outcome and actual outcome is computed downstream of the output neurons, and summarized by the scalar loss, L . For example, the loss could be the sum of squared error, $L = (1/2)\mathbf{e}^T\mathbf{e}$. The scalar loss signal, carried by the gold feedback path, is then globally broadcast to the network. Thus, each neuron receives the same feedback information about success on the task. When weight updates are based on the correlation between recent changes in the loss and recent node perturbations, these changes will on average be adaptive and reduce the loss. However, as the number of neurons in the network grows, these correlations become increasingly less informative and learning in large networks slows dramatically^{1,2}.



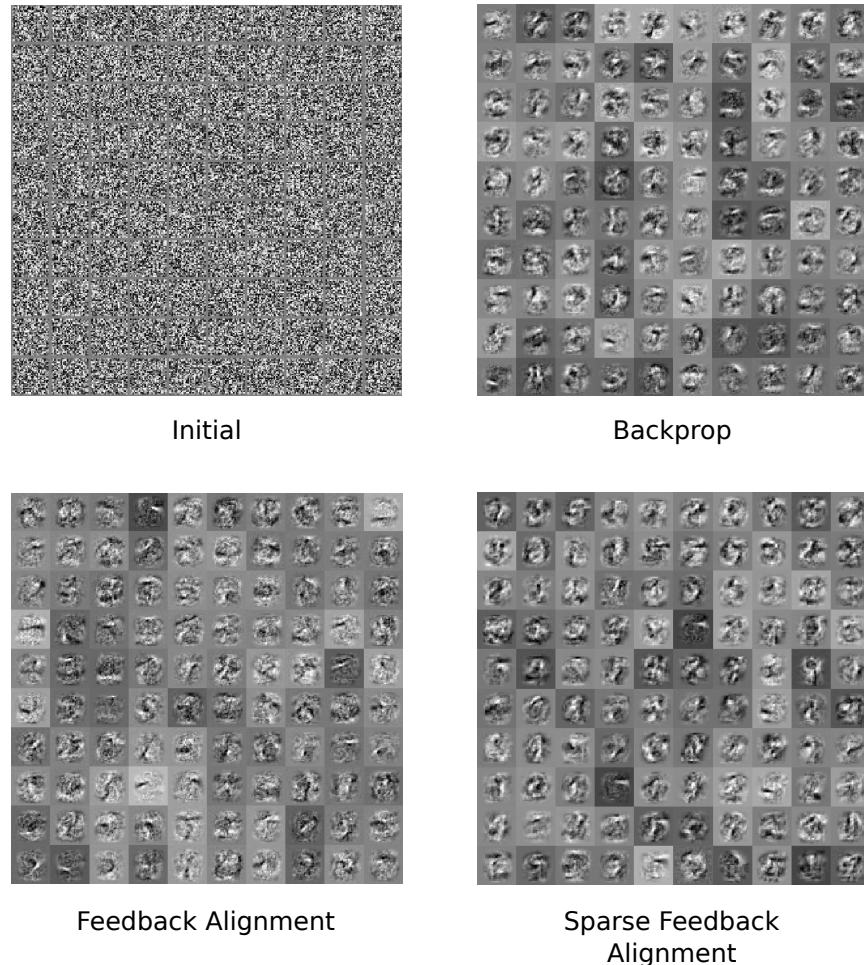
Supplementary Figure 2: Schematic of “shallow” learning in a multilayer network. The forward path is the same as in Figure 1. Error neurons (at bottom in gold) compute the difference between the network output, y , and a desired outcome, y^* , delivered by inputs arriving from the right hand side (in grey). That is, $e = y^* - y$. Each output neuron receives error information specifying its contribution to the loss, i.e. whether the neuron should reduce or increase its activity and by how much. Learning can be quick compared with reinforcement learning, but neurons deeper in the network receive no error information, and thus their representational power is wasted³, even in the case where earlier layers are initialized with unsupervised pretraining⁴.



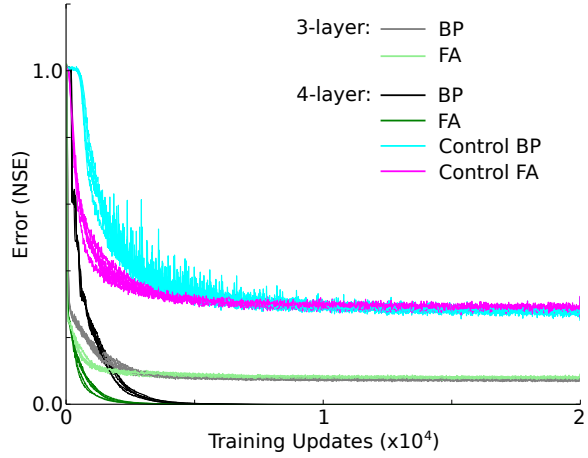
Supplementary Figure 3: Potential network architecture for feedback alignment. The forward and backward paths are the same as in Figure 2. However, in this case error neurons project to a set of feedback neurons through a synaptic matrix of random weights, B , to deliver modulatory signals, δ , to the hidden neurons. Note that in this case only one modulatory neuron connects to each neuron in the hidden layer. This is for diagrammatic purposes: feedback alignment works just as well if each modulatory neuron connects to many of the neurons in the hidden layer.



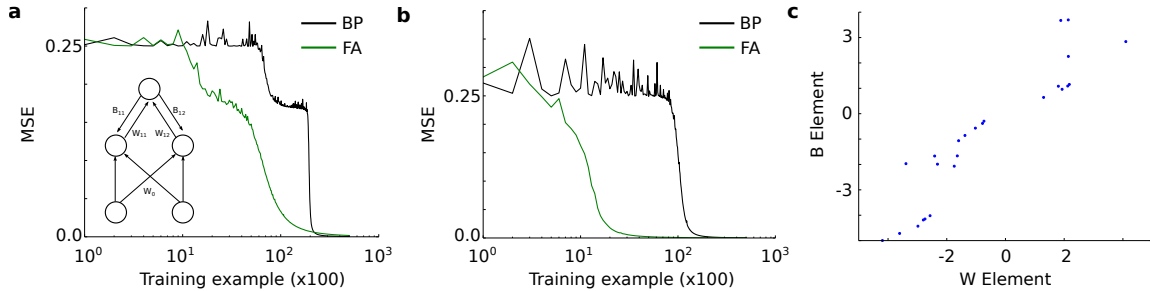
Supplementary Figure 4: Potential operation of feedback alignment with two hidden layers. Network structure is similar to that depicted in Figure 3, except that input units are not shown. In this case, error flows back through a second matrix of random weights to a corresponding set of feedback neurons. Ascending axon branches carry these error signals to the dendrites of the neurons in the deepest hidden layer, where they modulate learning.



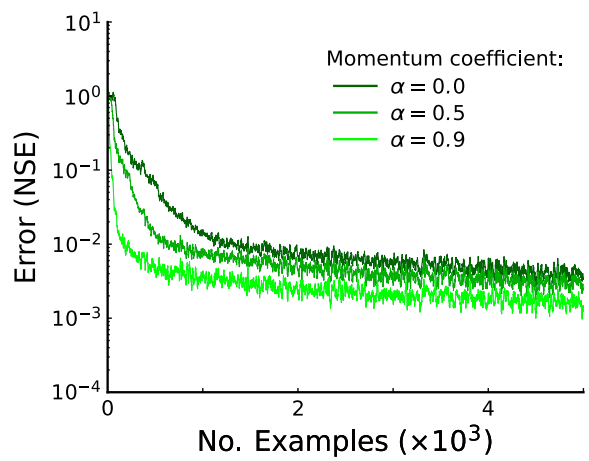
Supplementary Figure 5: Receptive fields for 100 randomly selected hidden units relating to Figure 3a-b in the main text. Receptive fields are shown at the beginning of learning (top left) and for the learning variants discussed in the main text. Grey scale indicates the strength of connection from each of 28×28 pixels in MNIST images. White denotes strong positive, black denotes strong negative.



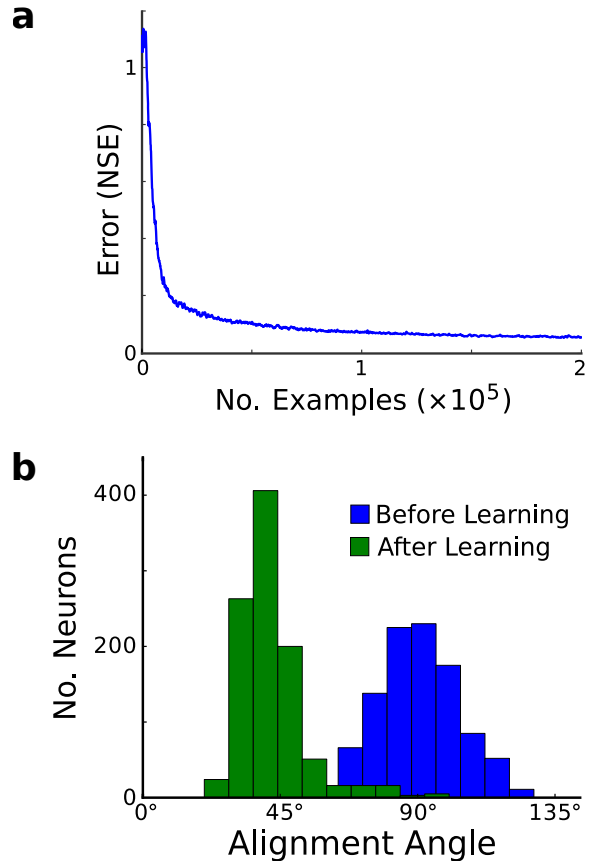
Supplementary Figure 6: Control experiment demonstrating that feedback alignment can send useful training signals to deeper layers. In control conditions (cyan and magenta), the first hidden layer of weights were held fixed. These networks performed significantly worse than in the cases where backprop or feedback alignment were used to update these weights (black and dark green). Data were derived from 5 runs of each experiment, each starting with a different initialization of all of the forward and backward weight matrices. NSE is normalized squared error.



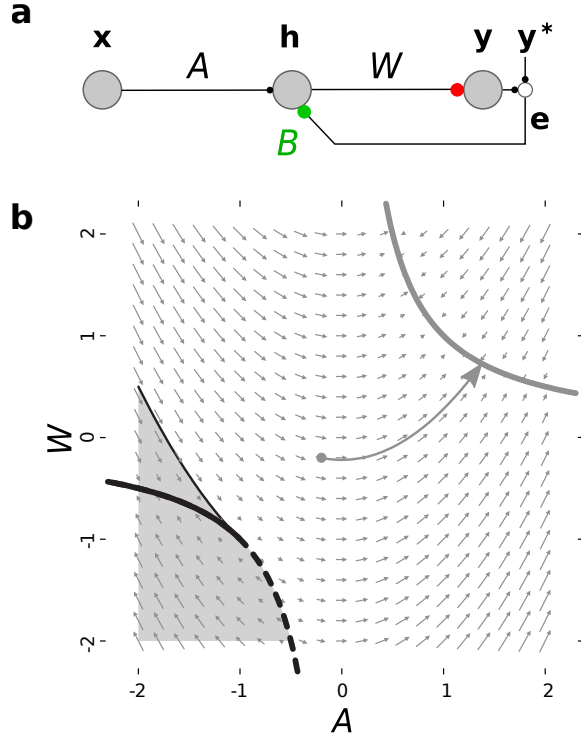
Supplementary Figure 7: Feedback alignment on the XOR problem. (a) Feedback alignment solves the classic XOR problem in a 2–2–1 network. MSE is mean squared error. (b) Feedback alignment solves the same problem in a 2–25–1 network. (c) Scatter plot of the 25 corresponding elements of the W and B matrices following the training shown in 'b'. Before training the elements are drawn from a normal distribution and the plot looks like an uncorrelated cloud.



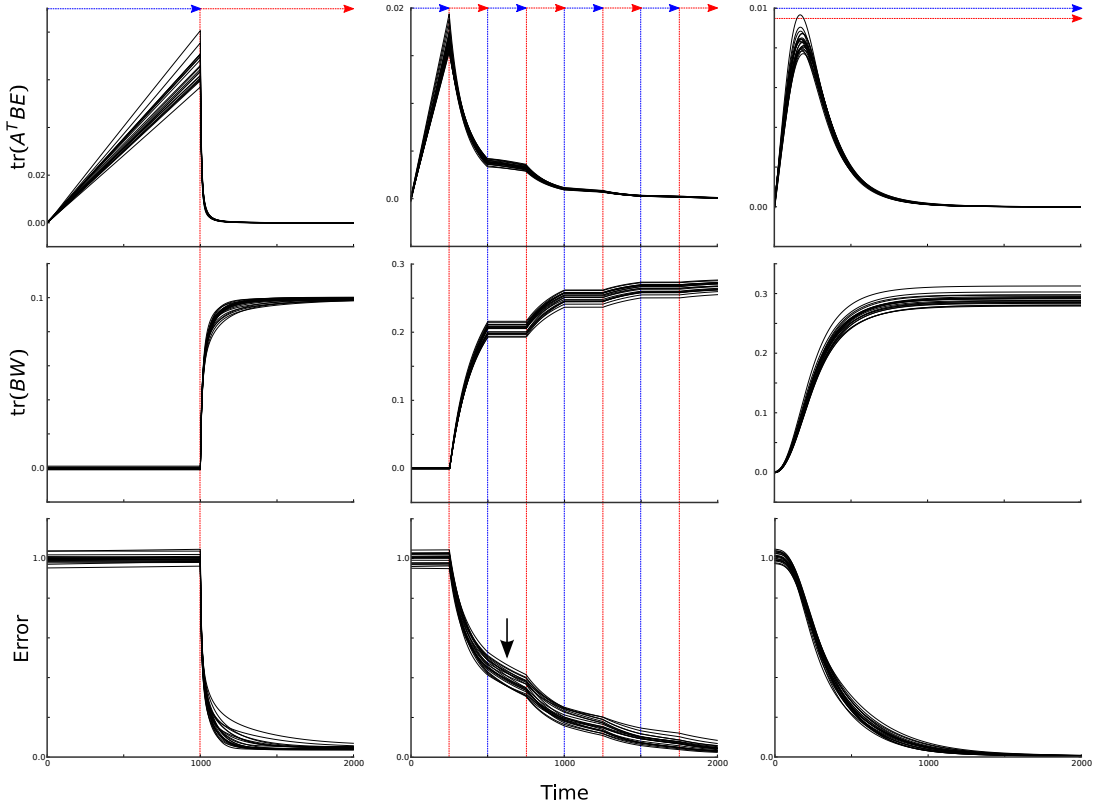
Supplementary Figure 8: Feedback alignment is sped up significantly by a simple momentum strategy.



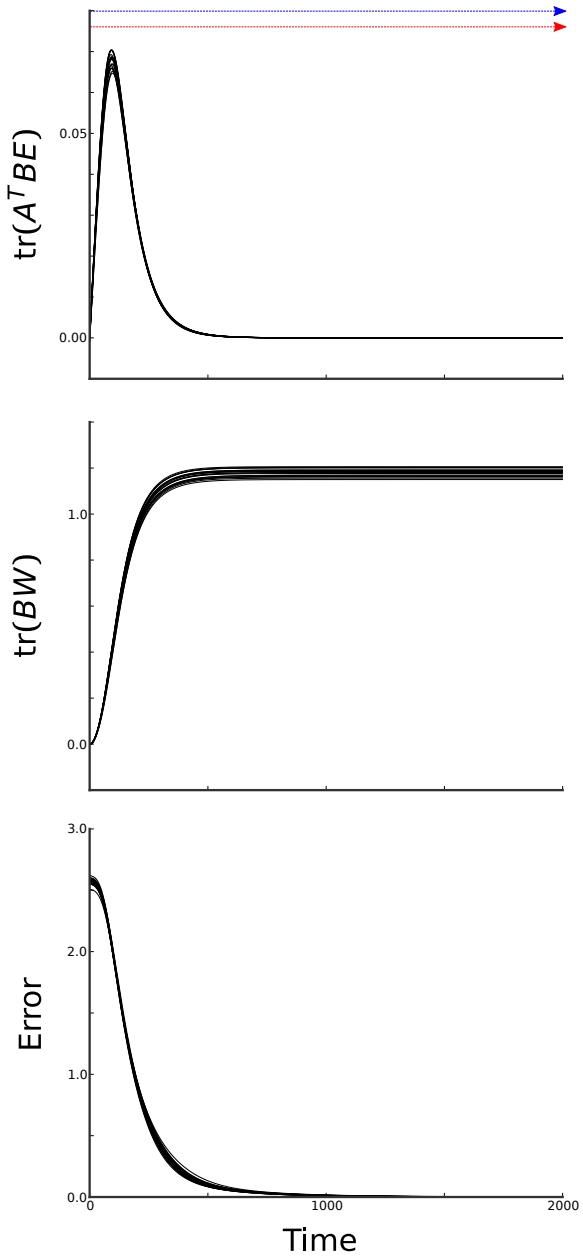
Supplementary Figure 9: Supplemental figure relating to Figure 5a in the main text. A $20 \times 1000 \times 20$ network learns to match a nonlinear target function via feedback alignment. **(a)** The normalized squared error (NSE) drops. **(b)** Histogram of the alignment of the angles between the forward and backward pathways for each hidden neuron. Before learning, these angles are unimodally and symmetrically distributed around 90° . After learning, this distribution shifts towards 0° i.e. the forward pathways have come to align with the random feedback paths on a neuron-by-neuron basis.



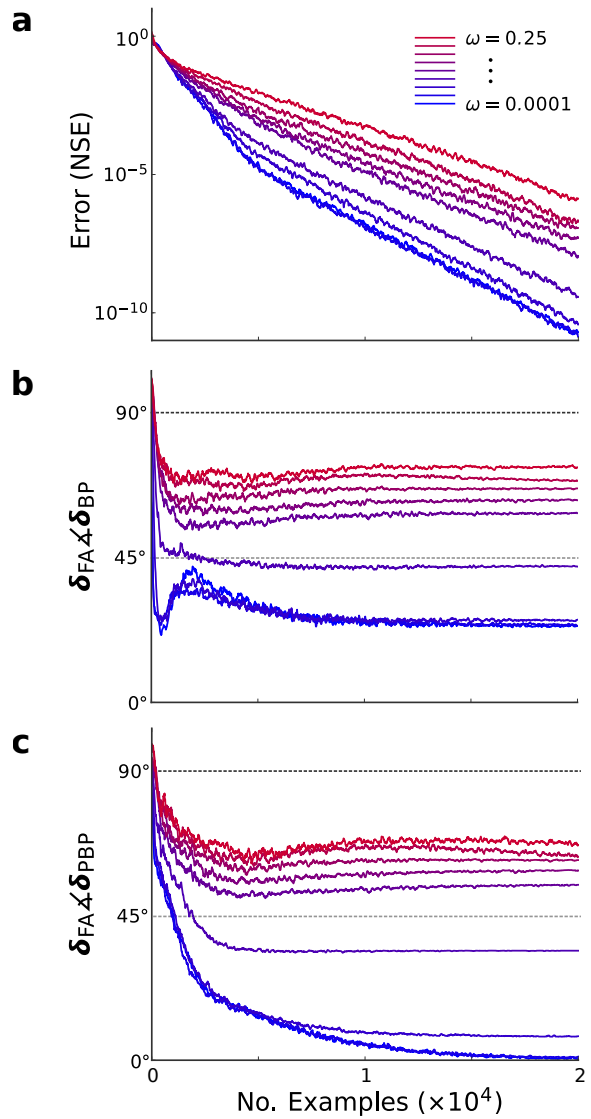
Supplementary Figure 10: Network dynamics underlying feedback alignment. **a**, Three-neuron network learning to match a linear function, $y^* = Tx$, with $T = 1$ and $B = 1$. **b**, Vector flow field (small arrows) demonstrates the evolution of A and W during feedback alignment. Thick lines are solution manifolds (i.e. $AW = 1 = T$) where: $eWBe > 0$ (grey), $eWBe < 0$ (black), or unstable solutions (dashed black). There is a small region of weight space (shaded grey) from which the system travels to the “bad” hyperbola at lower left, but this is simply avoided by starting near 0. Large arrow traces the trajectory for an initial condition where A and W were both initialized close to 0. To produce the flow fields, we computed the expected updates made by feedback alignment, yielding deterministic dynamics. Details for the deterministic dynamics are the same as in Proof #1 (Supplementary Note 11). The dynamics were simulated with custom-built code in Matlab. See Saxe et al. (2013) for instructive comparison with backprop’s dynamics in a similar three-neuron network⁵.



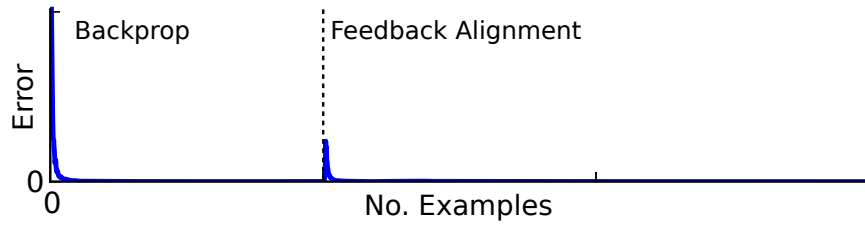
Supplementary Figure 11: A $30 \times 20 \times 10$ linear network is trained to match a linear function under 3 regimens (corresponding to the 3 columns). In the first column, we alternate a single time between learning in A (blue arrow), and then in W (red arrow). In the second column, we alternate multiple times between learning in A and W . In the third column, learning in A and W is synchronous. The networks were trained via the deterministic dynamics, and we repeated each simulation 20 times (black traces), each time starting with random weights and a random target function. During each learning trial we examined the 3 quantities, $\text{tr}(A^T BE)$, $\text{tr}(BW)$, and the error. In the first regime, when A is learned, there is very little change in the error, but $\text{tr}(A^T BE)$ quickly increases and becomes positive, indicating a buildup in alignment between A^T and BE . During this period, because W is held fixed, the alignment between B and W , measured by $\text{tr}(BW)$, remains small and close to zero. But, when learning in W begins, $\text{tr}(BW)$ quickly increases, indicating a buildup in alignment between B and W . The same essential story holds when we alternate between learning A and W many times. In this case, when we switch to learning in A for a second time, the teaching signals sent to A via B have become effective—error continues to drop even though W is not learning (black arrow). Although the magnitude of $\text{tr}(A^T BE)$ decreases over time, this is driven primarily by a decrease in the magnitude of the error. Importantly $\text{tr}(A^T BE)$ stays positive, indicating continued alignment between A^T and BE . Qualitatively the dynamics in the simultaneous case recapitulate those in the case of the decoupled dynamics. And, the described dynamics are qualitatively the same across all 20 repeated simulations in each regimen.



Supplementary Figure 12: A $100 \times 50 \times 20$ linear network is trained to match a linear function while we examine the quantities $\text{tr}(A^T BE)$, $\text{tr}(BW)$, and the error. We repeated each simulation 20 times (black traces), starting with random weights and a random target function. As in the third regimen in Figure 11, the weight matrices are updated simultaneously, and identical alignment trends are observed. With this larger network size the variance in the trajectories of these quantities is smaller (compare to Figure 11), as might be expected from the law of large numbers. Thus, feedback alignment tends to show less variance in the way that it performs as network size is increased.



Supplementary Figure 13: If A and W start small then W learns to act like a local pseudoinverse of B . **a**, Each trace is a single run of feedback alignment learning with the elements of A and W drawn uniformly from $[-\omega, \omega]$, where $\omega = [0.0001, 0.001, 0.01, 0.05, 0.1, 0.125, 0.15, 0.2, 0.25]$, corresponding to blue through red, respectively. Loss is normalized squared error (NSE). **b-c**, Angle between the hidden unit changes prescribed by feedback alignment versus backprop (panel b) and versus pseudobackprop (panel c).



Supplementary Figure 14: A network learns to match a quadratic function, as in the simulations for Figures 3a, 3c and 9. Initially the network learns with backprop. Once the network is close to a local minimum, the network is switched from learning with backprop to learning with feedback alignment. The error increases sharply following this switch. Thus, network parameters that minimize error need not correspond to equilibria of the dynamics induced by feedback alignment. Feedback alignment quickly recovers from the spike in error and finds a new network configuration with low error rates.

Supplementary Note 1. Architectures for different learning algorithms

We illustrate simple network architectures that can implement feedback alignment. To provide context, we first diagram the architectures of more familiar learning mechanisms: reinforcement learning (Figure 1) and “shallow” learning (Figure 2). We then illustrate feedback alignment in a network with a single hidden layer (Figure 3) and a network with two hidden layers (Figure 4). We emphasise that there are many possible network architectures that can support the operation of feedback alignment, but we think it is instructive to diagram at least one concrete example.

Supplementary Note 2. Extended computational results

In the main paper we showed that feedback alignment is effective in training relatively small networks. The question naturally arises whether feedback alignment can scale to more difficult problems. In a series of notes we discuss results for larger and deeper networks, and for bigger datasets, with reference to the machine learning literature. In general, we find that feedback alignment works about as well as backprop on these more difficult problems. We briefly discuss the selection of hyper-parameters, such as the scale of the backward matrices. As well, for didactic purposes, we briefly examine the classic XOR problem. Our results here are not exhaustive, but they show that feedback alignment scales well with network and problem size, and works with different kinds of data. Finally, we identify a kind of problem for which feedback alignment is limited: training networks that have very little redundancy in parameter space, e.g. deep, narrow autoencoders; feedback alignment has no difficulty training wide autoencoders. We speculate on why this limitation exists, and note that it does not pose a significant difficulty in the context of biological learning since there is little evidence of drastic parametric bottlenecks in the brain.

Most of the experiments described in this set of notes were run on a GPU and in minibatch mode with 100 samples per minibatch. In control experiments we saw no significant difference in the long-run performance of feedback alignment in single-sample versus minibatch modes. Thus, it appears that feedback alignment is equally applicable in batch mode and we therefore used minibatch mode to save time in many of the experiments. We used an NVIDIA GTX680 GPU card, which we accessed via the Cudamat and Gnumpy libraries^{6,7}.

Supplementary Note 3. Control experiment for training deeper layers

The experiments in Figure 3 of the main paper provide evidence that feedback alignment can take advantage of more than one layer of hidden units. However, it is possible that the performance gain observed in this figure might simply come from the fact that there are more

parameters in the network. To establish that feedback alignment is communicating useful error signals to the first layer, we examined the effect of freezing the first layer weights, W_0 . If observed performance gain was merely due to an increased number of hidden units or parameters, then feedback alignment would be expected to perform similarly under this control condition, as compared to when the first layer of weights are updated. Figure 6 shows that the 4-layer network with the frozen layer of weights performs much worse than the 4-layer network that is updated with feedback alignment (magenta versus dark green). The same pattern is observed when this control is performed with backprop (cyan versus black). Thus, we can conclude that feedback alignment, like backprop, is able to deliver useful training signals to the deeper hidden layer. Interestingly, performance for the controls was worse than in the 3-layer cases. This is because freezing W_0 induces random features at the first hidden layer, which are worse than using the raw inputs.

Unlike most of the experiments in these notes, these control experiments were run using TensorFlow⁸. Each training update used a minibatch of 100 examples. The forward and backward weights and biases of the target network and the learned networks were chosen from uniform distributions. The learning rate for all networks was 0.05. The target network architecture was: 30–20–10–10. The 3-layer network architecture was: 30–40–10. The 4-layer network architecture was: 30–40–20–10. The hidden layers used a $\tanh(\cdot)$ nonlinearity, and the output was linear. Inputs were drawn for a Normal distribution with $\mu = 0$ and $\sigma^2 = 1$.

Supplementary Note 4. The XOR problem

For didactic purposes, we briefly explore feedback alignment in the context of the classic XOR problem⁹. We trained a 2–2–1 network with both backprop and feedback alignment. Both algorithms used the same learning rate of 0.5 and both managed to find solutions to the XOR problem.

In this case, the forward output weight matrix was initialized to $(W_{11}, W_{12}) = (0.15, -0.13)$, the backward matrix was $(B_{11}, B_{12}) = (-3.75, -4.53)$. After training, the forward output weight matrix was $(W_{11}, W_{12}) = (-4.65, -4.55)$, coming into better alignment with the backward weight matrix. Figure 7a shows the learning curves for this experiment. To better visualize what happens during alignment, we also examined the XOR problem with a network with a larger hidden layer, 2–25–1.

In this case, the learning also works (Figure 7b) and we were able to compare the forward output weights and backward weights, before and after training. At initialization, there is no obvious relationship between the forward and backward weights, since both weights are chosen randomly. After training however, there is clear alignment of the forward and backward weights (Figure 7c). Note that while in these cases feedback alignment is quicker, one must be cautious in interpreting these results. In particular, while the learning rate is the same for both

algorithms, the scale of the backward matrix B can alter the effective learning rate of feedback alignment.

Supplementary Note 5. Extended results on MNIST

In the main paper (Figure 3a) we showed that feedback alignment successfully trains a network with a single hidden layer of 1000 units to classify MNIST digits. A single hidden layer network trained by feedback alignment on the permutation invariant version of MNIST achieved a test set error of 2.1%, which compares well with previous results under the same conditions¹⁰. The MNIST dataset is relatively dated, but it has been well studied and continues to be an important machine learning benchmark^{11,12,13}. We therefore explored various ways of improving performance on MNIST. Then we tested feedback alignment on the more recently developed SVHN dataset¹⁴.

We initially explored results for MNIST without any “augmentation” of the dataset or the model. Prior to the recent introduction of the dropout regularization strategy, the best reported result on the permutation invariant, unaugmented MNIST with a multilayer feedforward network, was 1.6% error on the test set^{15,12}. With backprop, using a 784–1500–1500–1500–10 network with $\tanh(\cdot)$ units we were able to replicate these past results, scoring 1.62% final error on the test set using our implementation. In these and all of the following experiments we used a simple learning rate schedule where η was reduced by an order of magnitude once progress had slowed substantially, e.g. from $\eta = 10^{-2} \rightarrow 10^{-3} \rightarrow 10^{-4}$. We employed a weight decay term of $\gamma = 10^{-6}$. For all classification tasks we normalized the inputs to have a mean of 0 and standard deviation of 1, and used a simple “1-hot” representation for the outputs with target values set to $\{-0.9, 0.9\}$ (see LeCun et al. 2012). We trained on the standard mean squared error of the outputs, ran five repeats of learning experiments, and report mean results.

With feedback alignment in the same network architecture we obtained 1.32% error on the test set and also converged in fewer minibatches than with backprop. We then explored various model and dataset augmentations. There are many known ways in which the results for MNIST can be improved upon using backprop. Foremost among these are:

1. using the rectified-linear unit (ReLU) activation function¹²: $f(x) = \max(0, x)$.
2. recently developed dropout regularization¹².
3. in contrast to the permutation invariant task, explicitly hard-wiring topological knowledge into the model, e.g. by using convolutional spatial filter layers¹⁰.
4. augmenting the dataset with additional data, e.g. via elastic distortions and translations of the images^{10,15}.
5. training multiple network models and averaging their results¹⁶.

6. generative or autoencoder pretraining^{17,18,19}.

We explored combining several of these approaches with feedback alignment. By employing dropout with feedback alignment (in a single hidden layer), the algorithm’s performance improved to 1.2% error on the test set. On the other hand, we found that direct use of the ReLu unit did not work well with feedback alignment—early learning before alignment takes place can push many of the units into the regime where $x < 0$, and therefore $f(x) = 0$ and there is no gradient. When this occurred, learning was no longer productive. However, a simple modification to a piece-wise linear function was effective, in which:

$$f(x) = \begin{cases} \frac{1}{20}x & : x \leq 0 \\ x & : x > 0 \end{cases} \quad (1)$$

By using this activation function (instead of $\tanh(\cdot)$) feedback alignment further reduced the test error to 1.1%.

We have not yet examined feedback alignment in conjunction with convolutional layers. Convolution networks require precise and quick weight transport, making them just as biologically implausible as standard implementations of backprop. This is because all of the neurons within a given convolutional map must share precisely the same receptive field¹⁰ (i.e. they have “tied weights”). This kind of weight sharing is known to be a particularly powerful kind of regularization^{10,15} for image data, but one that seems impossible for the brain to implement. Nevertheless, recent work has examined the performance of feedback alignment in the context of convolutional layers and finds that it struggles to perform well in this context²⁰. We believe that this is likely due to the fact that both weight sharing convolutions and feedback alignment are very strong regularizers. Feedback alignment is reliant on redundancy in the forward pathway in order to work, since the forward pathway needs to come into rough alignment with the backward path, whilst still solving the task. Since convolutional layers use substantial weight sharing, they have very little redundancy in their parameters and are thus likely to interact poorly with feedback alignment; we discuss this idea further in Section 9. We did try introducing a more plausible kind of topological knowledge that does not require weight transport into our network. We built a network in which the first layer consisted of 6 maps of neurons in which each neuron could “see” only a 6×6 patch of the presented image. Each neuron had its own receptive field weights and updated its weights independently of all the others; this is essentially a convolutional layer without weight sharing. Thus, the model incorporated topological information about the image, but did not share connections in a way that would require weight transport. Using this modification of the model, a 784–3174–1500–1500–10 network trained with feedback alignment obtained 0.8% on the test set. These experiments show that feedback alignment is able to take advantage of topological information built into the model.

We also augmented the training set by adding distorted versions of the training images. We deformed images using elastic distortions as previously described^{15,11}. By combining the previous model alterations with this dataset augmentation, feedback alignment gives 0.5%

error on the test set. Thus, feedback alignment is able to take advantage of this standard approach to improving backprop’s performance.

We also examined whether feedback alignment could function in even deeper networks. We trained a network with 10 hidden layers and 1000 units in each layer. In this case, we did not use any of the dataset or model augmentations. Feedback alignment reached 1.45% error on the MNIST test set in this case, and developed receptive fields in the first layer that were similar to those observed in other conditions, indicating that errors were effectively propagated by feedback alignment to even the deepest layers in the network. This network does not perform quite as well as the wider three hidden layer network trained with feedback alignment, but this might be expected since the 10 hidden layer network has many more parameters and may tend to overfit the data. The essential point is that gradient transmission is still effective in very deep networks. Training the same network with backprop gave an error of 1.65%.

We next examined the performance of feedback alignment on a more difficult variant of the MNIST dataset that is distributed by Yoshua Begio’s LISA website:

<http://www.iro.umontreal.ca/lisa/twiki/bin/view.cgi/Public/MnistVariations>.

In particular, we examined performance on the mnist-back-image variant of the dataset²¹. In this dataset, random patches from photographic images were used as the background for each MNIST digit, rendering much more complex images with a range of gray-scale values. For this task we examined performance for the standard training (50,000 images) and test set²¹ (10,000 images) with no model or dataset augmentation, but we used the larger set for training and the smaller set for testing. We trained a 784–1500–1500–1500–10 network of $\tanh(\cdot)$ units; backprop gave 21.5% on the test set error, and feedback alignment gave 20.66% error. Thus feedback alignment can match, and even exceed, backprop’s performance on more complicated data.

We note that feedback alignment’s result of 0.5% on the standard MNIST test set is not quite comparable with the state-of-the-art result of 0.23% error¹⁶, which used backprop training. However, these results make use of both model averaging and multiple layers of tied-weight convolutional units; convolutions in particular are known to make large improvements to MNIST results^{10,15}. Nevertheless, in some of the cases examined, feedback alignment gave improved performance on the test set relative to backprop. While this is not crucial to the central biological argument we make, we briefly speculate as to why this may sometimes occur.

In the cases where feedback alignment gave better final error on the test set, we suspect that the algorithm may be acting to regularize the forward parameters. As shown in Section 12, the forward path is implicitly pulled into alignment with the randomly chosen backward path. This constrains how the forward weight matrices can solve the classification problem. This soft constraint appears to act as a good regularizer for the MNIST problem—significantly better than weight decay, and about as good as dropout under the same conditions¹². We also found that in some cases feedback alignment gave speed increases over standard backprop, in the

sense that final error rates were reached with fewer minibatch presentations. The reason for this appears to be more straightforward. With feedback alignment, the delivery of errors to deeper layers is achieved via weights that are decoupled from the forward parameters. This means that it is straightforward to choose backward weights that propagate error effectively to all layers in the network, independent of changes in the forward weights. In our experiments we chose and fixed the random backward matrices, e.g. B_1, B_2, B_3 , so that roughly the same magnitude of error arrived at each layer. That is, the elements of each random backward weight matrix were drawn from the uniform distribution centred on zero and then the matrix was scaled by a constant to allow good gradient flow. In practice this is done very easily by trial and error. This makes it possible, in some sense, for feedback alignment to escape the vanishing gradient problems²² that make deep networks difficult to train²³. For example, if forward weights are initialized to be small, this will lead to very small gradients and slow learning in a network trained with backprop. In contrast, feedback alignment can still make quick progress in this situation because updates are not directly dependent on the scale of the forward weights (of course, it is possible to initialize the forward weights to be large, but this is usually undesirable¹⁸). It is too early to say whether this idea of decoupling forward and backward propagation can be used to leverage meaningful benefits in the current context of machine learning. There are many new algorithms and ideas that deal well with the vanishing gradient problem^{23,24,25}, and it is beyond the scope of the current work to offer a thorough analysis in terms of these approaches.

Supplementary Note 6. Results on the SVHN dataset

The Google Street View House Number (SVHN) dataset was developed in 2011 and consists of photographic images (32x32 pixels) of house numbers¹⁴. There are 604,388 images in the training set and 26,032 images in the test set, making it an order of magnitude larger than MNIST. The associated supervised task is to identify the digit in the centre of the image. The images are more complex than MNIST in a variety of ways. The images are larger than MNIST images (1024 versus 784 pixels). There is a variety of clutter in the images, both from random features in the environment and from other digits that are in view on either side of the central digit. There is substantial diversity among the camera angles and lighting conditions under which the images are taken. And, the pixel values span a wide range and are not limited to the black/white extremes typical of MNIST digits.

Previous work with the permutation invariant version of SVHN reports 10.3% classification error on the test set using a multilayer network of $\tanh(\cdot)$ units trained with backprop¹⁴. In this work the images were converted to grey-scale by taking the mean across the three colour channels. The network architecture used in the study was optimized by gridding over hyperparameters (e.g. layer size and learning rate), and the network was pretrained using a greedy layer-wise approach before backprop fine-tuning. We picked a single large network size and trained it with

feedback alignment on the same grey-scale images. With a 1024–3000–3000–3000–3000–10 network of $\tanh(\cdot)$ units feedback alignment gave 9.7% error. By introducing simple topological structure in the first layer (i.e. the same as in Section 5 but with 8 maps of neurons with 10x10 pixel receptive fields), feedback alignment improved to 8.1% error. And, by changing the hidden unit activation function to be piece-wise linear (as in Section 5), feedback alignment gave 7.1% error. Thus, our experiments demonstrate that, feedback alignment is capable of matching backprop on large, challenging datasets, and taking advantage of topological information built into the model. There are of course other manipulations which we have not yet examined. As with MNIST, multiple convolutional layers can be used to improve performance on SVHN²⁶. Additional performance gains can also come from dataset augmentation, using information available in the colour channels, and more sophisticated normalization techniques¹³.

Supplementary Note 7. Results on TIMIT data

The TIMIT is a corpus of read speech that has been phonetically transcribed. It contains recordings of 630 individuals from eight American English dialects reading predefined sentences with a variety of phonetic content. A frequently examined machine learning task is to predict the phoneme spoken in segments of audio in this corpus¹². We tested feedback alignment on a subset of the TIMIT dataset²⁷ for which the task is to classify input vectors as coming from one of six stop consonants. Each 10ms frame of audio is converted into Mel-frequency cepstral coefficients (MFCC) features, and the input data vectors are the concatenation of these vectors with the first two temporal derivatives of the MFCC features, to give a 39 dimensional input space²⁷. The training and test sets consist of 63881 and 22257 input/output pairs, respectively. On this task, in a 39–1000–1000–1000–6 network of $\tanh(\cdot)$ units, backprop achieved 24.3% error on the test set, while feedback alignment reliably performed better, giving 23.1% error. Thus, we find that feedback alignment is readily applicable to a variety of data types.

Supplementary Note 8. Feedback alignment with momentum

In the main text we used straightforward variants of backprop with a simple weight update scheme. Backprop training can be sped up in a variety of ways^{24,25,28}. Many of these require complex operations that are difficult to imagine the brain implementing. But some, such as momentum based strategies whereby weight updates build up speed in consistent directions^{29,28}, can offer substantial speed-ups while remaining simple enough that the brain might make use of them. We tested whether feedback alignment dynamics are compatible with momentum and whether the algorithm can be made quicker using such a strategy. We performed experiments with a 2-hidden layer network where the model and task were similar to those described for Figure 3d in the main text, except that parameter updates were governed by: $v_{t+1} = \alpha v_t + \Delta\theta_{FA}$,

and $\theta_{t+1} = \theta_t + v_t$, where α is the scalar momentum coefficient, v is the vector momentum term, $\Delta\theta_{FA}$ is the standard feedback alignment update at time-step t , and θ_t is the parameter vector at time-step t . We tried three values for the momentum coefficient: $\alpha = 0.0$, which is equivalent to standard feedback alignment, $\alpha = 0.5$, and $\alpha = 0.9$. We used the same network initialization and dataset sequence in each case. Momentum gave significant speed increases with feedback alignment (Figure 8). Thus, momentum does not interfere with the network dynamics that allow feedback alignment to make use of random feedback weights. Feedback alignment’s performance can be improved substantially via momentum and might be improved by other simple strategies for improving learning speed.

Supplementary Note 9. Limitations of feedback alignment

We have discovered one clear limitation of feedback alignment, although this does not effect its interest as a model for how learning might work in biological networks. Feedback alignment does not perform as well when there is significant lack of redundancy in the forward path parameters. For example, feedback alignment performs poorly on the problem of training deep, narrow autoencoder networks¹⁸, i.e. where the desired output of the network is its input vector. When such networks are made deep, and narrow in the middle, they have the potential to be used for data compression purposes¹⁸. We trained a 7 layer network, 784–1000–500–10–500–1000–784 composed of $\text{tanh}(\cdot)$ units to reconstruct MNIST digits. The standard 60000 image training set and 10000 image test set were used. The images were normalized to between -0.9 and 0.9. We examined the average squared reconstruction error on the test set. On this task, standard backprop produces significantly better results than feedback alignment when measured on the test set: backprop gives a test set error of 8.6 MSE, while feedback alignment gives 30.2 MSE. To demonstrate that it is not the task itself, but rather the narrowing of the network that it problematic for feedback alignment, we also trained a 784–1000–1000–1000–1000–1000–784 network—such that there was no bottle-neck constraint. With this architecture, feedback alignment gave 0.72 MSE on the test set, consistently outperforming backprop which gave 1.5 MSE. This second result tracks the classification results, which demonstrate that feedback alignment can act as a useful regularizer (Section 5). We speculate that feedback alignment struggles in the narrow case because there is too much constraint placed on the forward weights. At the location of the bottleneck, there are very few hidden units and thus very few random backward weights carrying gradient information into these units. The algorithm tries to find a setting of the forward weights that allow it to simultaneously solve the reconstruction problem, while making the gradients flowing into the 10 hidden units useful. With so little flexibility in the forward path at the bottle-neck, it seems that the constraint is too much and the network settles on a sub-optimal solution. This may be, in some sense, akin to setting a weight decay term much too high, causing a network to learn “too-smooth” an approximation of the target function. Thus, feedback alignment is limited in its applicability to deep networks that narrow substantially at intermediate layers. But there is little evidence for this

kind of dramatic narrowing and re-expansion of cell numbers in networks found in the brain, or other forms of significant parameter bottle-necking.

Supplementary Note 10. Analytic results

In the next set of notes we present three analytic results that provide insight into the efficacy of the feedback alignment algorithm and how it differs fundamentally from backprop. The first result gives conditions under which feedback alignment is guaranteed to reduce the error of a network function to 0 (Supplementary Note 11). The second result offers insight into how feedback alignment's dynamics drive the forward weights W to align with B^T , causing the error signals sent back through B to become meaningful (Supplementary Note 12). The third and fourth results both suggest a potential connection between the feedback alignment algorithm and the second-order Gauss-Newton method of error minimization. In the case of the fourth result, we provide conditions under which feedback alignment changes W so that it comes to align with B^+ , the Moore-Penrose pseudoinverse of B (Supplementary Note 14). Meanwhile, the third result shows how the backprop algorithm can be modified in a simple way, using W^+ in place of W^T , to implement an approximation of the Gauss-Newton method (Supplementary Note 15). A final note considers obstacles to a general proof of convergence for feedback alignment and shows that the dynamics induced by feedback alignment are non-conservative (Supplementary Note 16).

Supplementary Note 11. Condition for feedback alignment to zero error (Proof #1)

The empirical results presented in the main text and Supplemental Information suggest that the feedback alignment algorithm is effective across a broad range of problems. Although we cannot sharply delineate the space of learning problems where feedback alignment is guaranteed to work, we are able to establish a class of problems where feedback alignment is guaranteed to reduce training error to 0. Importantly this class of problems contains cases where useful modifications must be made to upstream synaptic weights to achieve this error reduction. Thus, we establish that feedback alignment does indeed succeed in transmitting useful error information to neurons deep within the network.

We consider a linear network that generates output \mathbf{y} , from input \mathbf{x} according to $\mathbf{y} = W\mathbf{h}$, with $\mathbf{h} = A\mathbf{x}$. For each data point \mathbf{x} presented to the network, the desired output, \mathbf{y}^* , is given by a linear transformation T so that $\mathbf{y}^* = T\mathbf{x}$, (T for target). Our goal is to modify the elements of A and W , so that the network is functionally equivalent to T .

Some comments on notation. Vectors \mathbf{x} , \mathbf{h} , \mathbf{y} , etc. are column vectors and we use standard matrix multiplication throughout. For example $\mathbf{x}^T \mathbf{x}$ is the inner product of \mathbf{x} with itself (resulting in a scalar) and $\mathbf{x}\mathbf{x}^T$ is the outer product of \mathbf{x} with itself (resulting in a matrix). For brevity

and clarity the matrices of synaptic weights referred to as W_0 and W in the main text are here referred to as A and W , respectively. When referring to the specific elements of A or W , we take A_i^j to be the weight from the i^{th} input element to the j^{th} hidden element, and similarly we take W_j^k to be the weight from the j^{th} hidden element to the k^{th} output element.

Importantly, the transport of error problem still applies even for a linear network, with a linear target function T , provided the number of output units is less than the number of hidden units, which is less than the number of input units, i.e. $n_o < n_h < n_i$. In this case the null space of A (those input vectors which A maps to zero) must be a subspace of the null space of T if the network function is to perfectly match the target function. The probability of a randomly initialized A having this property is zero. Thus, if feedback alignment is able to reduce error to zero, we can conclude that useful modifications have been made to A . Presumably, such modifications are only possible if useful information concerning the errors is employed when modifying A . In this note we prove that transmitting error information via a fixed arbitrary matrix, B , provides sufficiently useful information when updating A , to reduce error to zero.

For convenience we define $E = T - WA$, so that our error vector is $\mathbf{e} = Ex$. Then, the feedback alignment parameter updates can be written as

$$\Delta W = \eta E \mathbf{x} \mathbf{x}^T A^T \quad (2)$$

$$\Delta A = \eta B E \mathbf{x} \mathbf{x}^T. \quad (3)$$

Here, η is a small positive constant referred to as the learning rate.

Instead of modifying the parameters A and W after experiencing a single training pair $(\mathbf{x}, T\mathbf{x})$, it is possible to expose the network to many training examples, and then make a single parameter change proportional to the average of the parameter changes prescribed by each training pair. Learning in this way is called batch learning. In the limit, as batch size becomes large, parameter changes become deterministic and proportional to the expected change from a data point.

$$\Delta W = \eta [E \mathbf{x} \mathbf{x}^T A^T] \quad (4)$$

$$\Delta A = \eta [B E \mathbf{x} \mathbf{x}^T] \quad (5)$$

Here $[\cdot]$, denotes the expected value of a random variable. Under the assumption that the elements of \mathbf{x} are i.i.d. standard normal random variables (i.e. mean 0 and standard deviation 1), then $[\mathbf{x} \mathbf{x}^T] = I$. Here and throughout, I denotes an identity matrix. Thus, under this normality assumption, in the limit as batch size becomes large, the learning dynamics simplify to

$$\Delta W = \eta E A^T \quad (6)$$

$$\Delta A = \eta B E. \quad (7)$$

In the limit as the learning rate, η , becomes small, these discrete time learning dynamics converge to the continuous time dynamical system

$$\dot{W} = EA^T \quad (8)$$

$$\dot{A} = BE. \quad (9)$$

Our first result is in the context of this continuous time dynamical system.

Throughout the proof of our first result we will use the following relation

$$BW + W^T B^T = AA^T - C, \quad (10)$$

where C is a constant matrix. This follows from defining $C := BW + W^T B^T - AA^T$ and inspecting the derivative.

$$\dot{C} = B\dot{W} + \dot{W}^T B^T - \dot{A}A^T - A\dot{A}^T \quad (11)$$

$$= BEA^T + AE^T B^T - BEA^T - AE^T B^T \quad (12)$$

$$= 0 \quad (13)$$

We are now in a position to state and prove theorem 1.

Theorem 1. *Given the learning dynamics*

$$\dot{W} = EA^T \quad (8)$$

$$\dot{A} = BE, \quad (9)$$

if the constant C in equation 10 is zero and the matrix B satisfies $B^+B = I$, then

$$\lim_{t \rightarrow \infty} E = 0. \quad (14)$$

Some notes on the conditions of the theorem. Here and throughout, B^+ denotes the Moore-Penrose pseudoinverse of B . The condition $B^+B = I$ holds when the columns of B are linearly independent, and B has at least as many rows as columns, i.e. $n_o \leq n_h$. Note that if the elements of B are chosen uniformly at random, then the columns of B are linearly independent with probability 1. The condition $C = 0$ is met when $AA^T = BW + W^T B^T$. While there are many initializations of W , A and B that satisfy this condition, the only way to ensure that the $C = 0$ condition is satisfied for all possible B is for W and A to be initialized as zero matrices.

Proof. Our proof is loosely inspired by Lyapunov's method, and makes use of Barbălat's Lemma. Consider the quantity

$$V = \text{tr}(BEE^T B^T). \quad (15)$$

We use Barbălat's Lemma to show that $\dot{V} \rightarrow 0$.

Lemma 1 (Barbălat's Lemma). *If V satisfies:*

1. V is lower bounded,
2. \dot{V} is negative semi-definite,
3. \dot{V} is uniformly continuous in time, which is satisfied if \ddot{V} is finite,

then $\dot{V} \rightarrow 0$ as $t \rightarrow \infty$.

Because B and E are real valued, V is equivalent to $\|BE\|^2$. Here and throughout, $\|\cdot\|$ refers to the Frobenius norm. Consequently V is bounded below by zero, and so satisfies the first condition of Lemma 1.

Lemma 2. \dot{V} is negative semi-definite.

Differentiating equation 15, and using the linearity of the trace, its invariance under transposition, and equations 9 and 8 we have

$$\begin{aligned}\dot{V} &= \text{tr}(B\dot{E}E^T B^T + BE\dot{E}^T B^T) = \text{tr}(B\dot{E}E^T B^T) + \text{tr}(BE\dot{E}^T B^T) \\ &= 2\text{tr}(B\dot{E}E^T B^T) = 2\text{tr}(B(-\dot{W}A - W\dot{A})E^T B^T) \\ &= -2\text{tr}(BEA^T AE^T B^T) - 2\text{tr}(BWBEE^T B^T).\end{aligned}\tag{16}$$

Now, using equation 10 and the invariance of the trace under cyclic permutation and transposition,

$$\begin{aligned}2\text{tr}(BWBEE^T B^T) &= \text{tr}(BWBEE^T B^T) + \text{tr}(BWBEE^T B^T) \\ &= \text{tr}(BWBEE^T B^T) + \text{tr}(W^T B^T BEE^T B^T) \\ &= \text{tr}(AA^T(BEE^T B^T)) = \text{tr}(A^T BEE^T B^T A).\end{aligned}\tag{17}$$

Then,

$$\dot{V} = -2\text{tr}(BEA^T AE^T B^T) - \text{tr}(A^T BEE^T B^T A) \leq 0,\tag{18}$$

since each of these terms is of the form $\text{tr}(XX^T)$, i.e. the Frobenius norm of a matrix squared.

Lemma 3. A is bounded.

Define, $s = \text{tr}(AA^T)$. Then

$$\begin{aligned}\dot{s} &= 2\text{tr}(BEA^T) = 2\text{tr}(BTA^T - BWAA^T) \\ &= 2\text{tr}(BTA^T) - \text{tr}(AA^T AA^T).\end{aligned}\tag{19}$$

Now AA^\top is an $n_h \times n_h$ symmetric matrix and hence diagonalizable, therefore $s \leq n_h\lambda$, where λ is the dominant eigenvalue of AA^\top . Then $\text{tr}(AA^\top AA^\top) = \|AA^\top\|^2 \geq \lambda^2 \geq \left(\frac{s}{n_h}\right)^2$. It follows that $\dot{s} \leq 2\text{tr}(BTA^\top) - \left(\frac{s}{n_h}\right)^2$. Using the Cauchy-Schwarz inequality we have that

$$\text{tr}(BTA^\top)^2 \leq \text{tr}(AA^\top) \cdot \text{tr}(BTT^\top B^\top) = s\|BT\|^2, \quad (20)$$

so that when $s > \|BT\|^2$, then $\text{tr}(BTA^\top) \leq s$. Therefore $\dot{s} \leq 2s - \frac{s^2}{n_h^2}$ when $s > \|BT\|^2$. This implies that $\dot{s} \leq 0$ when $s > \|BT\|^2$ and $s > 2n_h$. We can conclude that for all time

$$s \leq \|BT\|^2 + 2n_h. \quad (21)$$

Lemma 4. \dot{V} is bounded.

Differentiating equation 18 we have that

$$\begin{aligned} \dot{V} &= -4\text{tr}(B\dot{E}A^\top AE^\top B^\top) - 4\text{tr}(BE\dot{A}^\top AE^\top B^\top) - 2\text{tr}(\dot{A}^\top BEE^\top B^\top A) - 2\text{tr}(A^\top B\dot{E}E^\top B^\top A) \\ &= 4\text{tr}(BEA^\top AA^\top AE^\top B^\top) + 4\text{tr}(BWBEA^\top AE^\top B^\top) - 4\text{tr}(BEBEA^\top AE^\top B^\top) \\ &\quad - 2\text{tr}(BEBEE^\top B^\top A) + 2\text{tr}(A^\top BEA^\top AE^\top B^\top A) + 2\text{tr}(A^\top BWBEE^\top B^\top A) \end{aligned} \quad (22)$$

Note that \dot{V} is expressed in terms of the traces of products of the matrices B , E , A , and BW , and the transposes of these matrices. B is constant so it is bounded. V is bounded below by zero, and $\dot{V} \leq 0$, so V must converge to some value, implying the E is bounded. Lemma 3 shows that A is bounded. Recall that $AA^\top = BW + W^\top B^\top$, and so A being bounded implies that BW and $W^\top B^\top$ are also bounded. Thus \dot{V} is also bounded.

The conditions of Lemma 1 hold and in the limit as $t \rightarrow \infty$, $\dot{V} \rightarrow 0$. Since both addends of \dot{V} have the same sign, in the limit both must be identically zero. In particular $\text{tr}(BEA^\top AE^\top B^\top) = 0$, therefore $BEA^\top = 0$. Here and for the remainder of this proof we use W , A , T and E to refer to the value of these matrices in the limit as $t \rightarrow \infty$. Since B is constant we have, $EA^\top = 0$.

Recall that $\dot{W} = EA^\top$, and so W is constant. Together with B being constant this implies that $AA^\top = WB + B^\top W^\top$ is also constant. By definition, $BEA^\top = BTA^\top - BWAA^\top$. Recall that $BEA^\top = 0$, and that B , W and AA^\top are all constant, and so BTA^\top must also be constant. Note that $A^\top = E^\top B^\top$, so a constant BTA^\top implies that $BTE^\top B^\top = 0$. Then we have

$$0 = BTE^\top B^\top = B^+ BTE^\top B^\top (B^+)^T = TE^\top = ET^\top. \quad (23)$$

By definition $EE^\top = ET^\top - EA^\top W^\top$, and since both addends are zero $EE^\top = 0$. Thus $\text{tr}(EE^\top) = \|E\|^2 = 0$ and E is identically zero. \square

Thus, in the linear case, we can identify conditions under which feedback alignment is guaranteed to reduce errors to zero. Importantly, the proof holds for cases where the error can

reach zero only if B transmits useful information to the hidden neurons. From the proof it is clear that the usefulness of B as a transmitter of teaching signals arises from complex implicit feedback dynamics. To visualize the phenomena described by the proof, we consider a minimal network with just one linear neuron in each layer (Figure 10a). We visualize (Figure 10b) how the network's two weights, A and W , evolve when the feedback weight B is set to 1. The flow field shows that the system moves along parabolic paths. From most starting points the network weights travel to the hyperbola at the upper right (Figure 10b). This hyperbola is a set of stable equilibria solutions where $W > 0$ and therefore $e^T W Be > 0$ for all e , which means W has evolved so that the feedback matrix B is delivering useful teaching signals. The proof demonstrates that high-dimensional analogues of the pattern of parabolic paths seen in the minimal network (Figure 10a-b), also hold for networks with large numbers of units. Indeed, the proof hinges on the fact that feedback alignment yields the relation $BW + W^T B^T = AA^T + C$, where C is a constant, i.e. the left-hand side is a quadratic function of A .

Supplementary Note 12. Intuitive explanation for alignment of W with B^T .

Across many experiments we find that the matrices W and B^T come to ‘align’ with each other in the sense that $\text{tr}(BW) > 0$.¹ The above proof establishes convergence in the linear case, but doesn’t offer a clear intuition about how feedback alignment works. And specifically, it does not illuminate the mechanism by which initially useless error signals transmitted through B come to provide useful learning signals for parameter changes in A . In this note we offer a formal analysis that suggests why W and B^T align with one another. We do this by decoupling the deterministic dynamics used in the preceding proof and tracking the time derivative of $\text{tr}(BW)$. We show that the time derivative of $\text{tr}(BW)$ tends to be positive, i.e. that feedback alignment increases the alignment between W and B^T . By decoupling we mean that first A learns on its own while W is frozen, and then W learns while A is frozen. This manipulation allows us to illustrate how information about the structure of B is incorporated into the structure of A , and how this information about B then flows from A into W , i.e. the learning rule for W implicitly incorporates aspects of B .

We begin by holding W fixed (i.e. $\dot{W} = 0$) and examining how A incorporates the structure of B via the learning dynamics:

$$\dot{A} = BE = BT - BWA \quad (24)$$

¹Note that $\text{tr}(BW) = [W]_{\downarrow} \cdot [B^T]_{\downarrow}$. We take $[\cdot]_{\downarrow}$ to be an operator which flattens a matrix into a vector. Thinking of W and B^T as vectors in a vector space—i.e., by simply flattening the matrices—then alignment means that the angle between these two vectors, $[W]_{\downarrow} \angle [B^T]_{\downarrow}$, drops below 90°.

Since W is a constant in this equation, A evolves according linear dynamics. We know that there are three ways this system can evolve through time:

1. The state converges to a fixed point, in which case the error converges to $\mathbf{0}$, since $\dot{A} \rightarrow \mathbf{0} \Rightarrow BE \rightarrow \mathbf{0} \Rightarrow E \rightarrow \mathbf{0}$. If we are in this case, then there is nothing left to consider since the system will obtain $\mathbf{0}$ error whether or not W and B align. Given straightforward random initializations of the system (i.e. the elements of A, B, W, T are all drawn i.i.d. from a Normal distribution), the probability of this case occurring is obviously small, and shrinks with increasing network size.
2. The state evolves to a cycle. Given random initializations of the system, this case will occur with probability 0. This can easily be seen in the case where A, B, W, T are all 2×2 matrices. For there to be a cycle in this case, the real part of the eigenvalues of BW must all be precisely 0.
3. The state A “blows up” or becomes exponentially large so that $\|A\|^2 = \text{tr}(A^T A)$ tends to increase. As expected, this is the only case we have observed in empirical experiments with networks of even moderate size. Thus, we will now examine this case more closely.

If $\text{tr}(A^T A)$ tends to grow, then on average, $d/dt \text{tr}(A^T A) > 0$. Now,

$$d/dt \text{tr}(A^T A) = 2\text{tr}(A^T \dot{A}) = 2\text{tr}(A^T BE), \quad (25)$$

so that on average $\text{tr}(A^T BE) > 0$, meaning that on average A is ‘aligned’ with BE .

Next, we hold A fixed, i.e. $\dot{A} = 0$ and examine the evolution of the quantity $d/dt \text{tr}(BW)$ given the dynamics

$$\dot{W} = EA^T. \quad (26)$$

Under these dynamics, we have that

$$d/dt \text{tr}(BW) = \text{tr}(BEA^T). \quad (27)$$

And, from above and the invariance of $\text{tr}(\cdot)$ to cyclic permutation, we have that

$$\text{tr}(BEA^T) = \text{tr}(A^T BE) > 0. \quad (28)$$

That is, $d/dt \text{tr}(BW)$ is positive, which means W is driven towards alignment with B . Thus, we see that the combined dynamics of \dot{A} and \dot{W} encourage W to align with B^T . This result is born out by experiments with the linear, batch version of the system described in proof #1 (Figures 11, 12). And, the same phenomenon is observed in nonlinear experiments (Figure 5 in the main text).

Supplementary Note 13. A closer look at feedback alignment dynamics

In the previous note we saw that feedback alignment's dynamics tend to drive W to align with B^T . However, feedback alignment updates do not converge with backprop (Figures 2b and 3b), superficially suggesting that δ_{FA} is merely a sub-optimal approximation of δ_{BP} . Further analysis shows that this view is too simplistic. Proof 1 says that weights A and W evolve to equilibrium manifolds, but simulations (Figure 13) and analytic results (Proof 2) hint at something more specific: that when the weights begin near 0, feedback alignment encourages W to act like a local pseudoinverse of B around the error manifold. This fact is important because if B were exactly W^+ (the Moore-Penrose pseudoinverse of W), then as we will show later, the network would be performing Gauss-Newton optimization for the hidden units. We call this update rule for the hidden units pseudobackprop, and will denote it by $\delta_{\text{PBP}} = W^+ \mathbf{e}$. We will describe its relation to backprop in detail below. Experiments with the 30–20–10 linear network show that the angle, $\delta_{\text{FA}} \angle \delta_{\text{PBP}}$ quickly becomes smaller than $\delta_{\text{FA}} \angle \delta_{\text{BP}}$ (Figure 13b–c). In other words feedback alignment, despite its simplicity, displays elements of second-order learning. The following notes further examine the connection between feedback alignment and learning with the pseudoinverse matrix.

Supplementary Note 14. B acts like the pseudoinverse of W (Proof #2)

Here we will prove that, under certain restricted conditions, feedback alignment's hidden unit update, $\delta_{\text{FA}} = B\mathbf{e}$, also satisfies

$$\delta_{\text{FA}} \propto W^+ \mathbf{e}. \quad (29)$$

This fact is important because, as we will show in the next note, updating the hidden unit with this learning rule is an approximation of the second order Gauss-Newton error minimization technique. Here we interpret ‘ \propto ’ unconventionally, taking it to mean that one quantity is a positive scalar multiple of the other, as contrasted with the conventional meaning where one quantity is a non-zero scalar multiple of the other.

Again we take a linear network which generates output \mathbf{y} , from input \mathbf{x} according to $\mathbf{y} = W\mathbf{h}$, with $\mathbf{h} = A\mathbf{x}$. We consider the dynamics of the parameters for this network when it is trained on a single input-output pair, $(\mathbf{x}, \mathbf{y}^*)$, using feedback alignment.

The dynamics of the network parameters under this training regime are

$$W_{t+1} = W_t + \Delta W_t \quad (30)$$

$$A_{t+1} = A_t + \Delta A_t, \quad (31)$$

with

$$\Delta W = \eta_W \mathbf{e} \mathbf{h}^T \quad (32)$$

$$\Delta A = \eta_A B \mathbf{e} \mathbf{x}^T. \quad (33)$$

As before, B is a random, fixed, matrix of full rank. η_W and η_A are small positive learning rates.

Because we only present the network with a single input, \mathbf{x} , we have that

$$\begin{aligned} \mathbf{h}_{t+1} &= A_{t+1} \mathbf{x} \\ &= (A_t + \Delta A_t) \mathbf{x} \\ &= \mathbf{h}_t + \eta_A B \mathbf{e} \mathbf{x}^T \mathbf{x} \\ &= \mathbf{h}_t + \eta_B \mathbf{B} \mathbf{e}. \end{aligned} \quad (34)$$

Here, $\eta_B = \mathbf{x}^T \mathbf{x} \eta_A$. For a judicious choice of η_A , namely $\eta_A = \eta_W / (\mathbf{x}^T \mathbf{x})$, we have $\eta_B = \eta_W = \eta$. For this choice of η_A it suffices to consider the simpler dynamics

$$W_{t+1} = W_t + \Delta W_t \quad (35)$$

$$\mathbf{h}_{t+1} = \mathbf{h}_t + \Delta \mathbf{h}_t \quad (36)$$

with

$$\Delta W = \eta \mathbf{e} \mathbf{h}^T \quad (37)$$

$$\Delta \mathbf{h} = \eta B \mathbf{e}. \quad (38)$$

These simplified dynamics exhibit interesting properties.

Lemma 5. *In the special case of W and A , and hence \mathbf{h} , initialized to zero, at every time step there is a scalar s_h such that*

$$\mathbf{h} = s_h B \mathbf{y}^* \quad (39)$$

and a scalar s_w such that

$$W = s_w \mathbf{y}^* (B \mathbf{y}^*)^T. \quad (40)$$

Proof. In the first time step, when $\mathbf{h} = 0$ and $W = 0$, the conditions 39 and 40 are trivially satisfied with $s_h = 0$ and $s_w = 0$. We note that when conditions 39 and 40 hold, we have that

$$\mathbf{y} = W \mathbf{h} = s_w s_h \mathbf{y}^* (B \mathbf{y}^*)^T (B \mathbf{y}^*) = s_y \mathbf{y}^*. \quad (41)$$

Here $s_y := s_w s_h (B \mathbf{y}^*)^T (B \mathbf{y}^*)$. Now,

$$\mathbf{e} = \mathbf{y}^* - \mathbf{y} = \mathbf{y}^* - s_y \mathbf{y}^* = (1 - s_y) \mathbf{y}^*. \quad (42)$$

Then

$$\Delta W = \eta \mathbf{e} \mathbf{h}^T = \eta(1 - s_y) s_h \mathbf{y}^* (B \mathbf{y}^*)^T \quad (43)$$

and

$$\Delta \mathbf{h} = \eta B \mathbf{e} = \eta(1 - s_y) B \mathbf{y}^*. \quad (44)$$

This yields

$$s_h^{t+1} = s_h^t + \eta(1 - s_y^t) s_h^t \quad (45)$$

and

$$s_w^{t+1} = s_w^t + \eta(1 - s_y^t) s_h^t. \quad (46)$$

By induction we can conclude that equations 39 and 40 hold for every time step. \square

Using the properties established by Lemma 5 we can prove the main result of this note.

Theorem 2. *Under the same conditions as Lemma 5, for the simplified dynamics described in equations 35 through 38, we have that the hidden unit updates prescribed by feedback alignment, $B\mathbf{e}$, are always a positive scalar multiple of $W^+\mathbf{e}$. That is*

$$sB\mathbf{e} = W^+\mathbf{e} \quad (47)$$

where s is a positive scalar.

Proof. From Lemma 5 we have that $W = s_w \mathbf{y}^* (B \mathbf{y}^*)^T$, with s_w a positive scalar, and that $\mathbf{e} = (1 - s_y) \mathbf{y}^*$, with $(1 - s_y)$ a positive scalar, so that $W^+\mathbf{e} = (1 - s_y) (s_w \mathbf{y}^* (B \mathbf{y}^*)^T)^+ \mathbf{y}^*$. Also from Lemma 5 we have that $\Delta \mathbf{h} = \eta(1 - s_y) B \mathbf{y}^*$. Thus it suffices to show that

$$sB\mathbf{y}^* = (\mathbf{y}^* (B \mathbf{y}^*)^T)^+ \mathbf{y}^*, \quad (48)$$

with s a positive scalar. We show this by manipulating the right hand side of equation 48.

$$\begin{aligned} (\mathbf{y}^* (B \mathbf{y}^*)^T)^+ \mathbf{y}^* &= (B \mathbf{y}^*)^{T+} \mathbf{y}^{*+} \mathbf{y}^* = B^{T+} \mathbf{y}^{*T+} \mathbf{y}^{*+} \mathbf{y}^* \\ &= B^{T+} \mathbf{y}^{*T+} \mathbf{y}^{*T} \mathbf{y}^{*T+} = B^{T+} \mathbf{y}^{*T+} \\ &= (B \mathbf{y}^*)^{T+} = sB\mathbf{y}^* \end{aligned} \quad (49)$$

Here $s = (B \mathbf{y}^*)^T (B \mathbf{y}^*)$. Note that s is a positive scalar. \square

Supplementary Note 15. Gauss-Newton modification of backprop (Proof #3)

Here we examine a method of deep learning which we refer to as pseudobackprop. Pseudobackprop consists of replacing the transpose matrix, W^T , with the Moore-Penrose pseudoinverse matrix, W^+ , in the backprop algorithm. Interestingly, as we demonstrate here, this update rule approximates Gauss-Newton optimization. Thus the pseudoinverse of the forward matrix, W^+ , not only satisfies the first condition from the main text, i.e. $\mathbf{e}^T W W^+ \mathbf{e} > 0$, it also prescribes second order updates for the hidden units.

Newton's method is a way of minimizing squared error. If $\mathbf{e}(\mathbf{h})$ is a vector valued error function of input \mathbf{h} , and $L(\mathbf{h}) = \frac{1}{2}\mathbf{e}(\mathbf{h})^T \mathbf{e}(\mathbf{h})$ is the scalar valued squared error, Newton's method finds the vector \mathbf{h}^* that minimizes L . It does this by starting with a guess of the value \mathbf{h}^* and iteratively improving this guess. The change in the guess, \mathbf{h} , prescribed by Newton's method is

$$\Delta \mathbf{h} = -L_{hh}^{-1} L_h^T \quad (50)$$

Here L_h and L_{hh} denote the first and second derivatives of L with respect to \mathbf{h} i.e. the gradient and the Hessian of L , respectively. Because L is the sum of squared errors, its Hessian can be written in terms of the first and second derivatives of \mathbf{e} with respect to \mathbf{h} .

$$L_h = \mathbf{e}^T \mathbf{e}_h \quad (51)$$

$$L_{hh} = \mathbf{e}_h^T \mathbf{e}_h + \mathbf{e}^T \mathbf{e}_{hh} \quad (52)$$

When the components of \mathbf{e} are small we have that $\mathbf{e}^T \mathbf{e}_{hh} \ll \mathbf{e}_h^T \mathbf{e}_h$, and thus the Hessian is approximately $L_{hh} \approx \mathbf{e}_h^T \mathbf{e}_h$. Using this approximation with Newton's method, yields the Gauss-Newton method which prescribes

$$\delta_{GN} = \Delta \mathbf{h} = -\left(\mathbf{e}_h^T \mathbf{e}_h\right)^{-1} \mathbf{e}_h^T \mathbf{e} = -\mathbf{e}_h^+ \mathbf{e}. \quad (53)$$

Now suppose we have a 3-layer network with input signal \mathbf{x} , weight matrices A and W , monotonic squashing function σ , hidden-layer activity vector $\mathbf{h} = \sigma(A\mathbf{x})$, linear output cells with activity,

$$\mathbf{y} = W\mathbf{h} = W\sigma(A\mathbf{x}), \quad (54)$$

and errors $\mathbf{e} = \mathbf{y}^* - \mathbf{y}$.

If we want to adjust \mathbf{h} using the Gauss-Newton method, the formula is

$$\delta_{GN} = \Delta \mathbf{h} = -\mathbf{e}_h^+ \mathbf{e} = W^+ \mathbf{e} \quad (55)$$

Most learning networks do not adjust activity vectors like \mathbf{h} , but rather synaptic weight matrices like A and W . Computing the Gauss-Newton adjustment to A is complicated, but a good

approximation is obtained by replacing W^T with W^+ in the backprop formula. That is, backprop says

$$\begin{aligned}
\Delta A_i^j &= -\eta \sum_k (\partial L / \partial \mathbf{e}^k) (\partial \mathbf{e}^k / \partial \mathbf{y}^k) (\partial \mathbf{y}^k / \partial A_i^j) = \eta \sum_k \mathbf{e}^k \partial \mathbf{y}^k / \partial A_i^j \\
&= \eta \sum_k \mathbf{e}^k \partial (\sum_{j'} W_{j'}^k \mathbf{h}^{j'}) / \partial A_i^j = \eta \sum_k \mathbf{e}^k \sum_{j'} W_{j'}^k \partial \mathbf{h}^{j'} / \partial A_i^j \\
&= \eta \sum_k \mathbf{e}^k \sum_{j'} W_{j'}^k \partial (\sigma(\sum_{i'} A_{i'}^{j'} \mathbf{x}^{i'})) / \partial A_i^j = \eta \sum_k \mathbf{e}^k \sum_{j'} W_{j'}^k D^{j'} \sum_{i'} \mathbf{x}^{i'} \partial A_{i'}^{j'} / \partial A_i^j \\
&= \eta \sum_k \mathbf{e}^k W_j^k D^j \mathbf{x}^i = \eta \sum_k \mathbf{e}^k W_k^T D^j \mathbf{x}^i.
\end{aligned} \tag{56}$$

Here D^j is the derivative of the squashing function, $\sigma(\cdot)$, evaluated at \mathbf{h}^j . Note that $\partial_{i'}^{j'}/\partial A_i^j$ is zero except when $i' = i$ and $j' = j$.

Replacing W^T by W^+ in the last line of equation 56, we have

$$\Delta A_i^j = \eta \sum_k \mathbf{e}^k W_k^+ D^j \mathbf{x}^i \tag{57}$$

This adjustment yields a change in \mathbf{h} that approximates the Gauss-Newton one, recall equation 55. To see this, note that under pseudobackprop

$$\Delta \mathbf{h}^j = \sigma(\sum_i (A_i^j + \Delta A_i^j) \mathbf{x}^i) - \sigma(\sum_i A_i^j \mathbf{x}^i). \tag{58}$$

Applying a first order Taylor approximation of σ about $\sum_i A_i^j \mathbf{x}^i$ we have

$$\begin{aligned}
\Delta \mathbf{h}^j &\approx \mathbf{h}^j + D^j (\sum_i (A_i^j + \Delta A_i^j) \mathbf{x}^i - A_i^j \mathbf{x}^i) - \mathbf{h}^j \\
&= D^j \sum_i \Delta A_i^j \mathbf{x}^i = \eta (D^j)^2 \sum_i (\mathbf{x}^i)^2 \sum_k \mathbf{e}^k W_k^+ D^j \mathbf{x}^i \\
&= \eta (D^j)^2 \mathbf{x}^T \mathbf{x} \boldsymbol{\delta}_{GN}^j.
\end{aligned} \tag{59}$$

That is, each element of the pseudobackprop adjustment to the hidden units is, to first order, the Gauss-Newton adjustment, times a positive scalar, $\eta (D^j)^2 \sum_i (\mathbf{x}^i)^2$. Thus, if η is chosen to be $1/(D^j)^2 \sum_i (\mathbf{x}^i)^2$, pseudobackprop is exactly Gauss-Newton minimization for the hidden units.

In the context of training an artificial network, pseudobackprop may be of little interest. The pseudoinverse matrix is expensive to compute, so clock cycles can be better spent either by simply taking more steps using the transpose matrix, or by using more efficient second order methods.

Supplementary Note 16. Obstacles to a general convergence proof

We have considered various aspects of feedback alignment's operation, but it remains an open question as to what can be proved for the general non-linear version of the algorithm. This is perhaps unsurprising given that even the dynamics of learning in deep linear networks with backprop have only recently been studied in depth⁵. Here we provide insight into why a general proof must be radically different from those used to demonstrate convergence for backprop. Proofs of the convergence of backprop make use of the fact that the parameter dynamics induced by backprop follow the gradient of the loss function^{30,31,29}. In this note we will show that, in contrast, the dynamics induced by feedback alignment are not the gradient of any function, let alone the loss function. Thus, while feedback alignment is found to be effective in practice, and our formal analyses of the linear case offer insight into its mechanism, the details of the nonlinear case remain to be fully explored.

We begin by recalling the non-linear dynamics of both backprop and feedback alignment. We consider a network function parameterized by weight matrices A and W and by output and hidden layer biases b and c . The network makes use of a squashing function σ . We compare the dynamics of these parameters under backprop and feedback alignment. Our network function is defined by

$$\mathbf{y} = W\mathbf{h} + \mathbf{b} \quad (60)$$

$$\mathbf{h} = \sigma(\mathbf{a}) \quad (61)$$

$$\mathbf{a} = A\mathbf{x} + \mathbf{c}. \quad (62)$$

The parameter updates are derived from performance on a training set \mathcal{X} of pairs $(\mathbf{x}, \mathbf{y}^*)$. For a given training pair we define the error, $\mathbf{e} = \mathbf{y}^* - \mathbf{y}$. The point loss, a function of the parameters $\theta = (A, W, \mathbf{b}, \mathbf{c})$ and a particular training pair is $L(\theta, \mathbf{x}, \mathbf{y}^*) = \frac{1}{2}\mathbf{e}^T \mathbf{e}$. The total loss is then

$$\mathcal{L}(\theta) = \sum_{(\mathbf{x}, \mathbf{y}^*) \in \mathcal{X}} L(\theta, \mathbf{x}, \mathbf{y}^*). \quad (63)$$

As discussed above, both backprop and feedback alignment can be run online, with parameter updates based on the point loss, L , from a single training example, or in batch mode with parameter updates based on the total loss, \mathcal{L} . For simplicity, we consider the standard gradient descent style. With backprop the parameter updates are precisely proportional to the gradient

of the loss evaluated at the current parameters, $\nabla \mathcal{L}|\theta$, i.e.

$$\Delta W = \eta \sum_{\chi} \mathbf{e} \mathbf{h}^T = \eta \sum_{\chi} -\frac{\partial L(\theta)}{\partial W} \quad (64)$$

$$\Delta \mathbf{b} = \eta \sum_{\chi} \mathbf{e} = \eta \sum_{\chi} -\frac{\partial L(\theta)}{\partial \mathbf{b}} \quad (65)$$

$$\Delta A = \eta \sum_{\chi} ((W^T \mathbf{e}) \odot D) \mathbf{x}^T = \eta \sum_{\chi} -\frac{\partial L(\theta)}{\partial A} \quad (66)$$

$$\Delta \mathbf{c} = \eta \sum_{\chi} W^T \mathbf{e} = \eta \sum_{\chi} -\frac{\partial L(\theta)}{\partial \mathbf{c}}. \quad (67)$$

Here we use \odot to denote element-wise multiplication of vectors or matrices, and as before D denotes the derivative of the squashing function σ evaluated at a .

In the limit as the learning rate, η , becomes small this discrete time dynamical system converges to the continuous time dynamic system

$$\dot{\theta} = -\nabla \mathcal{L}. \quad (68)$$

In other words the vector flow field of the parameters is the gradient of the loss function. This ensures that the dynamics of the parameters constantly decrease the loss, and that as a result the local minimum, θ^* , of \mathcal{L} are precisely the asymptotically stable fixed points of the dynamical system backprop induces on θ . This basic fact serves as the starting point for proofs concerning the convergence of backprop^{30,31,29}.

Now consider the dynamics prescribed by feedback alignment.

$$\Delta W = \eta \sum_{\chi} \mathbf{e} \mathbf{h}^T \quad (69)$$

$$\Delta \mathbf{b} = \eta \sum_{\chi} \mathbf{e} \quad (70)$$

$$\Delta A = \sum_{\chi} ((B \mathbf{e}) \odot D) \mathbf{x}^T \quad (71)$$

$$\Delta \mathbf{c} = \sum_{\chi} (B \mathbf{e}) \odot D \quad (72)$$

A proof of the efficacy of feedback alignment would ideally give necessary and sufficient conditions under which the induced dynamics reduce the loss $\mathcal{L}(\theta)$ to a local minimum, θ^* , or to within a neighbourhood of a local minimum. A straightforward way to construct such a proof is to find a function, say $\mathcal{F}(\theta)$, such that two conditions are met. First, the minima of $\mathcal{F}(\theta)$ bear some relation to the minima of $\mathcal{L}(\theta)$, and second, the dynamics induced on θ by feedback

alignment are equal to the gradient of $\mathcal{F}(\theta)$. If we could find such an \mathcal{F} , feedback alignment's dynamics would drive θ to a minimum, and we could examine the relationship between the minima of \mathcal{F} and \mathcal{L} .

However, such a straightforward approach can never work. The dynamics induced by feedback alignment are non-conservative, i.e. the changes it prescribes for θ are not the derivative of any function of θ . Whilst this is true of the general case, it can be most readily seen in the scalar linear case, i.e. where the weight matrices W and A , and the feedback matrix B are scalars, and the bias vectors b and c are also scalars b and c , and where σ is simply the identity.

Suppose that there is a real-valued function \mathcal{F} , such that

$$(\dot{W}, \dot{b}, \dot{A}, \dot{c}) = \nabla \mathcal{F}(\theta) = \left(\frac{\partial \mathcal{F}}{\partial W}, \frac{\partial \mathcal{F}}{\partial A}, \frac{\partial \mathcal{F}}{\partial b}, \frac{\partial \mathcal{F}}{\partial c} \right). \quad (73)$$

The second derivative of \mathcal{F} in this case is

$$\frac{\partial^2 \mathcal{F}}{\partial \theta \partial \theta} = \begin{pmatrix} \frac{\partial \mathcal{F}}{\partial W \partial W} & \frac{\partial \mathcal{F}}{\partial W \partial A} & \frac{\partial \mathcal{F}}{\partial W \partial b} & \frac{\partial \mathcal{F}}{\partial W \partial c} \\ \frac{\partial \mathcal{F}}{\partial b \partial W} & \frac{\partial \mathcal{F}}{\partial b \partial A} & \frac{\partial \mathcal{F}}{\partial b \partial b} & \frac{\partial \mathcal{F}}{\partial b \partial c} \\ \frac{\partial \mathcal{F}}{\partial A \partial W} & \frac{\partial \mathcal{F}}{\partial A \partial A} & \frac{\partial \mathcal{F}}{\partial A \partial b} & \frac{\partial \mathcal{F}}{\partial A \partial c} \\ \frac{\partial \mathcal{F}}{\partial c \partial W} & \frac{\partial \mathcal{F}}{\partial c \partial A} & \frac{\partial \mathcal{F}}{\partial c \partial b} & \frac{\partial \mathcal{F}}{\partial c \partial c} \end{pmatrix}. \quad (74)$$

This matrix, like all Hessian matrices, is symmetric since $\frac{\partial \mathcal{F}}{\partial W \partial A} = \frac{\partial \mathcal{F}}{\partial A \partial W}$, etc.

Now consider the updates, $\dot{\theta}$, actually induced by feedback alignment. It suffices to consider the update for a single (scalar) pair, (x, y^*) , in the training set.

$$\dot{W} = eh \quad (75)$$

$$\dot{b} = e \quad (76)$$

$$\dot{A} = Bex \quad (77)$$

$$\dot{c} = Be. \quad (78)$$

Differentiating these updates with respect to the parameters we have

$$\begin{aligned}
\frac{d}{d\theta} \dot{\theta} &= \begin{pmatrix} \frac{d}{dW} eh & \frac{d}{db} eh & \frac{d}{dA} eh & \frac{d}{dc} eh \\ \frac{d}{dW} e & \frac{d}{db} e & \frac{d}{dA} e & \frac{d}{dc} e \\ \frac{d}{dW} Bex & \frac{d}{db} Bex & \frac{d}{dA} Bex & \frac{d}{dc} Bex \\ \frac{d}{dW} Be & \frac{d}{db} Be & \frac{d}{dA} Be & \frac{d}{dc} Be \end{pmatrix} \\
&= \begin{pmatrix} h^2 & -h & -Wxh + ex & -W + e \\ -h & -1 & -Wx & -W \\ -Bhx & -Bx & -BWx^2 & -BWx \\ -Bh & -B & -BWx & -BW \end{pmatrix}. \tag{79}
\end{aligned}$$

This derivative is not symmetric and hence the dynamics prescribed by feedback alignment are not the gradient of any function, i.e. the dynamics are non-conservative. This means that unlike proofs about backprop, proofs about feedback alignment cannot be based on a straightforward guarantee of eventual and consistent reduction of any function quantity, let alone training loss.

Another way to conceptualize this difficulty is to consider the dynamics induced by feedback alignment on the parameters at a local minimum, θ^* , of the loss, \mathcal{L} , in the case that this local minimum does not achieve precisely zero error on the training set. In this case, the changes prescribed will drive the parameters away from the local minimum, θ^* , and, at least in the short term, increase the loss. The only exception to this occurs when the feedback matrix B is such that $\sum_{\mathcal{X}} ((Be) \odot D)x^T = 0$. In general, the minima of \mathcal{L} , excluding those with zero error over the training set, will not be fixed points of the dynamics induced by feedback alignment. This issue is illustrated in Figure 14, where the loss over a training set is first taken to a local minimum by the backprop algorithm, and after this local minimum is achieved we switch to feedback alignment dynamics.

Supplementary References

- [1] Seung, H. S. Learning in spiking neural networks by reinforcement of stochastic synaptic transmission. *Neuron* **40**, 1063–1073 (2003).
- [2] Werfel, J., Xie, X. & Seung, H. S. Learning curves for stochastic gradient descent in linear feedforward networks. *Neural Computation* **17**, 2699–2718 (2005).
- [3] Bengio, Y. & LeCun, Y. Scaling learning algorithms towards AI. In Léon, B., Olivier, C., DeCoste, D. & Weston, J. (eds.) *Large Scale Kernel Machines* (MIT Press, 2007).

- [4] Lamblin, P. & Bengio, Y. Important gains from supervised fine-tuning of deep architectures on large labeled sets. In *Neural Information Processing Systems*, vol. 24th of *Deep Learning and Unsupervised Feature Learning Workshop*, 1–8 (2010).
- [5] Saxe, A. M., McClelland, J. L. & Ganguli, S. Exact solutions to the nonlinear dynamics of learning in deep linear neural networks. *arXiv preprint arXiv:1312.6120* (2013).
- [6] Mnih, V. Cudamat: A cuda-based matrix class for python. Tech. Rep. UTML TR 2009-004, University of Toronto (2009).
- [7] Tielemans. Gnumpy: an easy way to use GPU boards in python. Tech. Rep. UTML TR 2010-002, University of Toronto (2010).
- [8] Abadi, M. et al. TensorFlow: Large-scale machine learning on heterogeneous systems (2015). URL <http://tensorflow.org/>. Software available from tensorflow.org.
- [9] Rumelhart, D. E., McClelland, J. L., Group, P. R. et al. *Parallel distributed processing*, vol. 1 (IEEE, 1988).
- [10] LeCun, Y., Bottou, L., Bengio, Y. & Haffner, P. Gradient-based learning applied to document recognition. In *Proceedings of the IEEE*, vol. 86, 2278–2324 (1998).
- [11] Ciresan, D., Meier, U., Gambardella, L. & Schmidhuber, J. Deep big simple neural nets for handwritten digit recognition. *Neural Computation* **22**, 3207–3220 (2010).
- [12] Hinton, G. E., Srivastava, N., Krizhevsky, A., Sutskever, I. & Salakhutdinov, R. R. Improving neural networks by preventing co-adaptation of feature detectors. *arXiv preprint arXiv:1207.0580* (2012).
- [13] Wan, L., Zeiler, M., Zhang, S., Cun, Y. L. & Fergus, R. Regularization of neural networks using dropconnect. In *Proceedings of the 30th International Conference on Machine Learning (ICML-13)*, 1058–1066 (2013).
- [14] Netzer, Y. et al. Reading digits in natural images with unsupervised feature learning. In *NIPS workshop on deep learning and unsupervised feature learning*, vol. 2011, 4 (2011).
- [15] Simard, P., Steinkraus, D. & Platt, J. C. Best practices for convolutional neural networks applied to visual document analysis. In *ICDAR*, vol. 3, 958–962 (2003).
- [16] Ciresan, D., Meier, U. & Schmidhuber, J. Multi-column deep neural networks for image classification. In *Computer Vision and Pattern Recognition (CVPR), 2012 IEEE Conference on*, 3642–3649 (IEEE, 2012).
- [17] Hinton, G., Osindero, S. & Teh, Y. A fast learning algorithm for deep belief nets. *Neural Computation* **18**, 1527–1554 (2006).
- [18] Hinton, G. & Salakhutdinov, R. Reducing the dimensionality of data with neural networks. *Science* **313**, 504–507 (2006).

- [19] Bengio, Y. & Thibodeau-Laufer, É. Deep generative stochastic networks trainable by backprop. *arXiv preprint arXiv:1306.1091* (2013).
- [20] Liao, Q., Leibo, J. Z. & Poggio, T. How important is weight symmetry in backpropagation? *arXiv preprint arXiv:1510.05067* (2015).
- [21] Larochelle, H., Erhan, D., Courville, A., Bergstra, J. & Bengio, Y. An empirical evaluation of deep architectures on problems with many factors of variation. In *Proceedings of the 24th international conference on Machine learning*, 473–480 (ACM, 2007).
- [22] Bengio, Y., Simard, P. & Frasconi, P. Learning long-term dependencies with gradient descent is difficult. *Neural Networks, IEEE Transactions on* **5**, 157–166 (1994).
- [23] Glorot, X. & Bengio, Y. Understanding the difficulty of training deep feedforward neural networks. In *International Conference on Artificial Intelligence and Statistics*, 249–256 (2010).
- [24] Martens, J. Deep learning via hessian-free optimization. In *ICML-27*, 735–742 (Haifa, Israel, 2010).
- [25] Duchi, J., Hazan, E. & Singer, Y. Adaptive subgradient methods for online learning and stochastic optimization. *The Journal of Machine Learning Research* **12**, 2121–2159 (2011).
- [26] Sermanet, P., Chintala, S. & LeCun, Y. Convolutional neural networks applied to house numbers digit classification. In *Pattern Recognition (ICPR), 2012 21st International Conference on*, 3288–3291 (IEEE, 2012).
- [27] Cotter, A., Srebro, N. & Keshet, J. A gpu-tailored approach for training kernelized svms. In *Proceedings of the 17th ACM SIGKDD international conference on Knowledge discovery and data mining*, 805–813 (ACM, 2011).
- [28] LeCun, Y. A., Bottou, L., Orr, G. B. & Müller, K.-R. Efficient backprop. In *Neural networks: Tricks of the trade*, 9–48 (Springer, 2012).
- [29] Phansalkar, V. & Sastry, P. Analysis of the back-propagation algorithm with momentum. *IEEE Transactions on Neural Networks* **5**, 505–506 (1994).
- [30] White, H. Learning in artificial neural networks: A statistical perspective. *Neural computation* **1**, 425–464 (1989).
- [31] Tesauro, G., He, Y. & Ahmad, S. Asymptotic convergence of backpropagation. *Neural Computation* **1**, 382–391 (1989).